ORNL/TM-2016/237
Revision: 0

Severe Accident Analysis of BWR Core Fueled with UO_2/FeCrAl with Updated Materials and Melt Properties from Experiments

Fuel Cycle Research & Development
Advanced Fuels Campaign

K. R. Robb
J. W. McMurray
K. A. Terrani

Prepared for
U. S. Department of Energy
Office of Nuclear Energy

June 2016
M2FT-16OR020205042

ORNL/TM-2016/191
Revision 0

M2FT-16OR020205042: Severe Accident Analysis of BWR Core Fueled with UO_2/FeCrAl with Updated Materials and Melt Properties from Experiments

K. A. Robb
J. W. McMurray
K. A. Terrani

June 2016

Prepared by
OAK RIDGE NATIONAL LABORATORY
Oak Ridge, TN 37831-6283
managed by
UT-BATTELLE, LLC
for the
US DEPARTMENT OF ENERGY
under contract DE-AC05-00OR22725

INTENTIONALLY BLANK

ABSTRACT

Iron-chromium-aluminum (FeCrAl) alloys are being considered as advanced fuel cladding concepts with enhanced accident tolerance. FeCrAl alloys have slower oxidation kinetics and higher strength compared to Zr-based alloys at high temperatures. FeCrAl could be used for fuel cladding and spacer or mixing vane grids in light water reactors and/or as channel box material in boiling water reactors (BWRs). There is a need to assess the potential gains afforded by the FeCrAl accident tolerant fuel concept over the existing zirconium based materials employed today.

To accurately assess the response of FeCrAl alloys under severe accident conditions, a number of FeCrAl properties and characteristics are required. These include thermophysical properties such as density, thermal conductivity, specific heat, and melting points, as well as burst characteristics, oxidation kinetics, possible eutectic interactions, and failure temperatures. Oak Ridge National Laboratory (ORNL) has pursued refined values for the melting point of FeCrAl metal and the oxide formed by FeCrAl. This investigation included both experimental tests and modeling predictions. The melting point of several FeCrAl alloys and oxides of those alloys were interrogated using Differential Scanning Calorimetry (DSC) and Thermal Arrest analyses. The solidus temperatures of the metals with Fe-Cr-Al compositions were determined and compare well with reported data for commercial FeCrAl alloys. The oxides of failed FeCrAl specimens showed no DSC peak indicative of melting up to 1700°C in Ar-20%O_2 atmosphere.

Using refined properties for FeCrAl, the severe accident performance of a BWR plant utilizing FeCrAl fuel cladding and channel boxes was assessed using the MELCOR code. A range of station blackout severe accident scenarios were simulated for a BWR/4 reactor with Mark I containment. Overall, when compared to the traditional Zircaloy-based cladding and channel box system, the FeCrAl concept may provide a few extra hours of time for operators to take mitigating actions and/or for evacuations to take place. A coolable core geometry is retained longer, enhancing the ability to stabilize an accident. Finally, due to the slower oxidation kinetics, less hydrogen is generated, and the generation is delayed in time. This decreases the amount of non-condensable gases in containment and the potential for deflagrations to inhibit the accident response.

INTENTIONALLY BLANK

CONTENTS

Page

LIST OF FIGURES

Page

LIST OF TABLES

Page

INTENTIONALLY BLANK

M2FT-16OR020205042: Severe Accident Analysis of BWR Core Fueled with UO_2/FeCrAl with Updated Materials and Melt Properties from Experiments

1. INTRODUCTION

The US Department of Energy (DOE) Fuel Cycle Research and Development Advanced Fuels Campaign is leading the research, development, and demonstration of nuclear fuels with enhanced accident tolerance, known as accident-tolerant fuels (ATFs) [1]. By definition, ATFs are fuels and/or cladding that, in comparison with the standard urania fuel–Zr-based alloy cladding system, can tolerate loss of active cooling in the core for a considerably longer time period while maintaining or improving the fuel performance during normal operations. It is important to note that the currently used urania–Zr-based cladding fuel system tolerates design basis accidents (and anticipated operational occurrences and normal operation) as prescribed by the US Nuclear Regulatory Commission (NRC). There are three major potential approaches for the development of ATFs:

- improved fuel properties
- improved cladding properties to maintain core coolability and retain fission products, and
- reduced rate of reaction kinetics with steam to minimize enthalpy input and hydrogen generation.

One proposed ATF concept is based on iron-chromium-aluminum alloys (FeCrAl) [2,3]. With respect to enhancing accident tolerance, FeCrAl alloys have substantially slower oxidation kinetics compared to the zirconium alloys typically employed. During a severe accident, FeCrAl would tend to generate heat and hydrogen from oxidation at a slower rate compared to the zirconium-based alloys in use today.

1.1 PROGRESSION OF ATF ANALYSES

As materials development of ATF concepts progress, there has been a parallel effort in the analysis of the ATF performance and their gains with respect to the urania fuel–Zr-based alloy cladding system in use today. Over time, these analyses have been refined as the ATF concepts matured and more accurate thermophysical properties became available.

Early during the development of the ATF concept, scoping simulations of the plant response were performed under a range of accident scenarios using various ATF cladding concepts and fully ceramic microencapsulated fuel (FCM). Design basis loss of coolant accidents (LOCAs) and station blackout severe accidents were analyzed at Oak Ridge National Laboratory (ORNL) for boiling water reactors (BWRs) [4]. Researchers investigated the effects of thermal conductivity on design basis accidents [5], silicon carbide (SiC) cladding [6], neutronic feedback of FCM fuel [7], design basis accidents with uranium nitride fuel [8], as well as the effects of ATF concepts on the late stage accident progression [9]. These preliminary analyses were performed to provide initial insight into the possible improvements that ATF concepts could provide and to identify issues with respect to modeling ATF concepts. In addition to these scoping studies, screening studies were performed [10] and a common methodology and set of performance metrics were developed to compare and support prioritizing ATF concepts [11].

More recently, preliminary analyses for a few ATF concepts were evaluated during LOCA and severe accident scenarios for the CPR1000 pressurized water reactor (PWR) [12].

1.1.1 BWR Station Blackout Analysis Progression

The first study [4], of the FeCrAl ATF concept during station blackout (SBO) severe accident scenarios in BWRs was based on simulating short term SBO (STSBO), long term SBO (LTSBO), and modified SBO scenarios occurring in a BWR-4 reactor with MARK-I containment. The analysis indicated that FeCrAl had the potential to delay the onset of fuel failure by approximately 2.5-6 hours depending on the scenario, and it could delay lower head failure by approximately 7-7.5 hours. The analysis

demonstrated reduced in-vessel hydrogen production. However, the work was preliminary and was based on limited knowledge of material properties for FeCrAl. Limitations of the MELCOR code were identified for direct use in modeling ATF concepts. The effort also used an older version of MELCOR (1.8.5).

A second study [13] used an updated BWR model for MELCOR 1.8.6 [14] and more representative material properties for FeCrAl. The analysis included unmitigated SBO scenarios (LTSBO and STSBO) as well as mitigated SBO scenarios where water injection was restored to stabilize the accident. In all scenarios analyzed, the FeCrAl ATF concept provided gains over the existing Zircaloy system currently in use.

For the unmitigated SBO scenarios, the gains are in the form of delaying the accident progression and decreasing the amount of flammable gases generated. The delays ranged from tens of minutes to a few hours (about 4.5h) of additional time. Substantially less flammable and non-condensable gasses were generated: 0.6–13.7 tons less by the end of the simulation, depending on the scenario, and the timing of generation was delayed. The FeCrAl ATF concept provided an additional 1–4.4 hours of time (depending on scenario) before radionuclide release to the environment.

The results of the mitigated SBO scenarios illustrated the potential benefits of the delayed accident progression and decreased loads on containment. In all three cases analyzed using the FeCrAl ATF concept, the accident was stabilized within 32 hours without deflagrations occurring in the building or releases of radionuclides to the environment. In contrast, for two of the cases employing Zircaloy, the containment failed, deflagrations occurred in the reactor building, and radionuclides were released into the environment. Containment was predicted not to fail for one Zircaloy case; however, the loads on containment were predicted to be quite high. The simulations demonstrated the advantage of FeCrAl for enhancing the accident tolerance of a plant by affording an opportunity to mitigate and stabilize a severe accident.

1.1.2 Current Study of BWR SBOs

This report is an extension of the two previous studies. The purpose of the study is to provide refined estimates of the potential gains afforded by the FeCrAl ATF concept during BWR SBO scenarios. This study covers refined values for the metallic FeCrAl melt point and better informed melting and relocation characteristics of the oxidized FeCrAl. The efforts to determine the melting points are discussed in Section 2. Previously, the low temperature oxidation rate equation for FeCrAl (<1500°C) was implemented over the full range of temperature. The current study models the rapid oxidation of FeCrAl at temperatures above 1773 K (1500°C). Similar to the previous analyses, unmitigated and mitigated SBO accident scenarios are considered. Section 3 describes the accident scenarios chosen, figures of merit used in the comparison, MELCOR code, plant model, and the modeling of FeCrAl in MELCOR. The results for the SBO accident scenarios are discussed in Section 4. Finally, the findings and suggested future work are discussed in Section 5.

2. EXPERIMENAL WORK IN SUPPORT FOR THE PARAMETRIC DESIGN OF THE SIMULATIONS

2.1 BACKGROUND

Melting behavior of fuel and cladding systems are crucial data for simulating reactor behavior under severe accident scenarios. While FeCrAl alloys have been in use for many years, only approximate solidus temperatures are available in white papers for only a few commercial compositions, for example APM [15] and APMT [16]. For the oxides that form as scale on the base metal or that exist in more significant amounts after high temperature steam exposure, the situation is even worse. Only sparse literature data can be found regarding melting behavior of the binary subsystems of the integral Fe-Cr-Al-O quaternary. The aim of the experimental portion of this work is to determine the solidus temperatures for accident tolerant FeCrAl cladding alloys and their oxides.

2.2 MELTING OF METAL ALLOYS

2.2.1 Sample preparation

Square sections approximately 6 mm by 6 mm with a thickness of 1.3 mm were cut using a Buehler Isomet low speed saw from six rolled plates of FeCrAl alloys prepared at ORNL and summarized in Table 1. The specimens were then hot mounted to an aluminum disk with crystal bond, ground by hand with P# 1000 SiC paper using a Struers RotoPol-22 polishing wheel rotating at 300 rpm with water as a lubricant to remove the surface oxide layer. After extraction from the mount, they were flipped over, remounted, and the polishing procedure was repeated. Finally, the specimens were freed from the bonding, cleaned with acetone to eliminate any residue, and the mass of each was determined using a Sartorius Genius balance.

Table 1. Specimen labels and corresponding compositions in wt% of the FeCrAl alloys studied in this work

Alloy	Fe	Cr	Al	Y	C	S	O	N
B107Y	83.1	9.98	6.87	0.039	0.001	0.001	0.0015	0.0005
B166Y	77.86	16.06	6.06	0.003	0.003	0.0023	0.0014	0.0004
B058Y	87.16	5.04	7.73	0.037	0.003	0.0013	0.0012	0.0003
B008Y	92.14	0	7.83	0.012	0.006	0.0016	0.0014	0.0026
B085Y	87	8.05	4.87	0.064	0.001	0.0007	0.0017	0.0003
B005Y	95.1	0	4.84	0.032	0.005	0.0012	0.0015	0.002

2.2.2 Experimental procedure

A thermal arrest method was used to determine solidus for each of the alloys discussed above with an STA 449 F1 Jupiter from Netzsch-Gerätebau GmbH, Selb, Germany. The details of these measurements are well described in numerous other works, for example in [17]. In brief, as a pure substance melts, any heat energy is consumed by the solid to liquid isothermal phase transformation. For multicomponent systems, such as the alloys investigated in this study, there is a change in the temperature vs enthalpy relationship. In both cases, the onset of melting manifests as an interruption in the temperature-time profile for a given heating rate and was determined in this work using the Proteus companion analysis software for the STA 449 F1 Jupiter.

The thermocouples were calibrated using melting points for five different metal standards listed in Table 2 provided.

2.2.3 Results

A representative temperature profile showing the thermal arrest due to alloy B107Y traversing the solidus is shown in Figure 1. Each sample was melted and solidified three times; the solidus was taken as an average of the three temperatures upon heating since undercooling upon solidification is a common problem for many materials including those studied here. Complete results are given in Table 3.

Table 2. Reported purity of the melting standard used for the STA 449 F1 Jupiter thermocouple temperature calibration

Material	Purity (%)
Ni	99.99
Al	99.999
Zn	99.999
Au	99.999
Ag	99.99

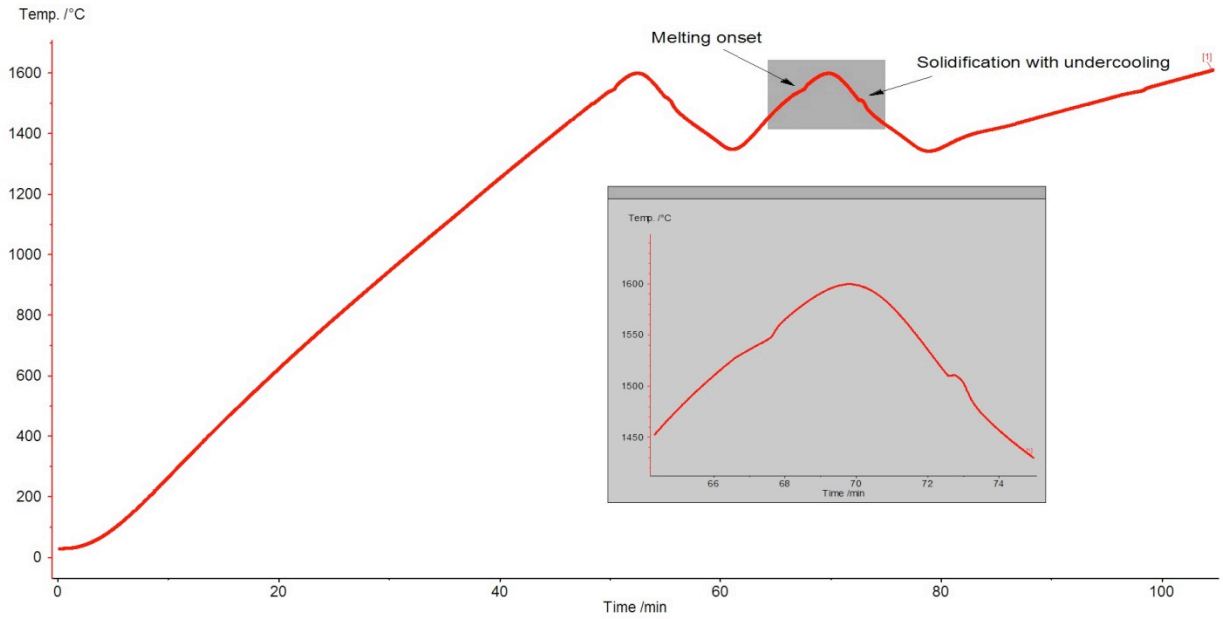

Figure 1. Thermal arrest results for alloy B107Y.

Table 3. Tabulated results of solidus measurements for the alloys studied in this work

Alloy	Solidus Temperature (°C)
B107Y	1528.9
B166Y	1525.9
B058Y	1533.1
B008Y	1538.5
B085Y	1532.4
B005Y	1543.4

While Figure 2 shows reasonable agreement between the measured melting results and those calculated using the preliminary CALPHAD thermodynamic assessment of Fe-Cr-Al from this work, it should be pointed out that the models that comprise the Fe-Cr-Al ternary assessment were developed based on the Fe-Cr, Fe-Al, and Cr-Al binary assessments from [18], [19], and [20] assuming no ternary interactions. This is a simplification, due to previous lack of data; however, the agreement can now be improved with the experimental solidus data generated in this study.

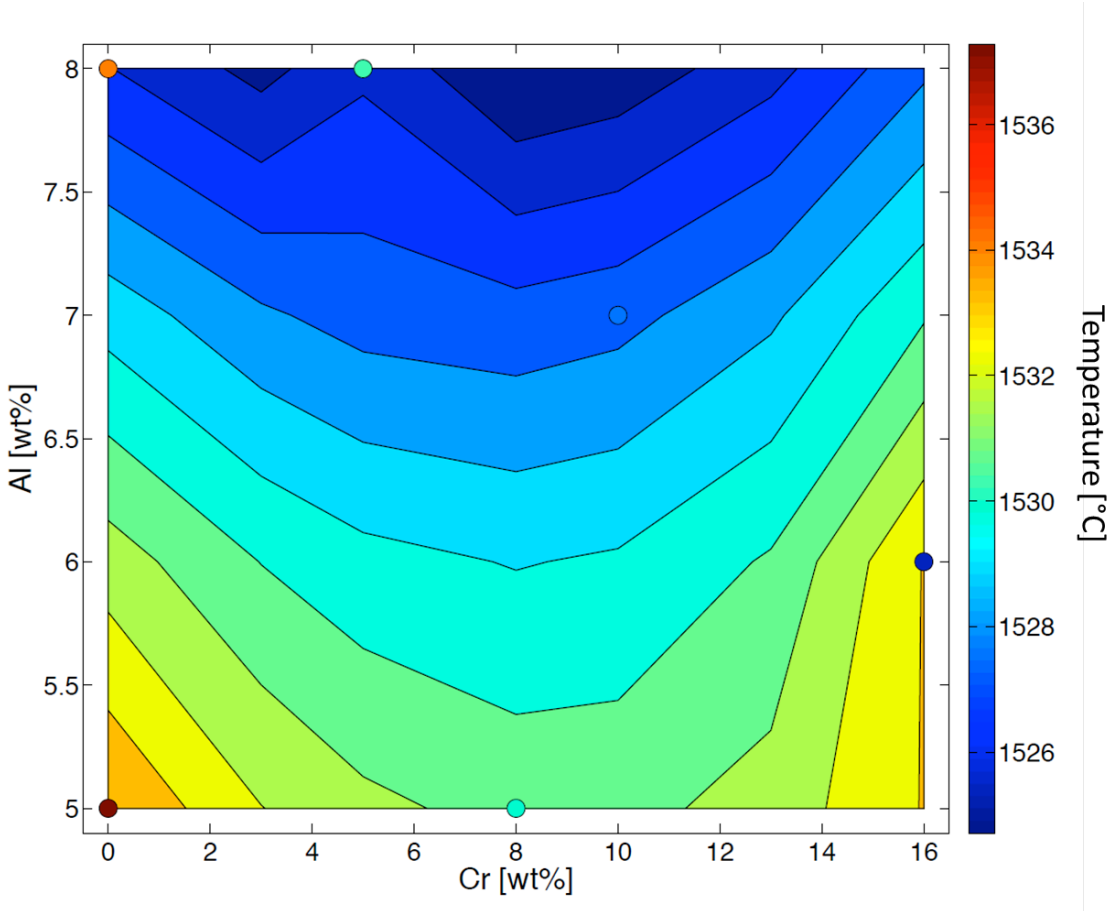

Figure 2. Comparison of experimental solidus temperatures for FeCrAl alloys as a function of Al and Cr content to those computed using the thermodynamic models developed in this work.

2.3 PHASE STABILITY OF THE OXIDES

2.3.1 Sample preparation

Various FeCrAl alloys are systematically exposed to 100% steam and varying temperature ramps in a Rubotherm thermogravimetric rig at ORNL's Severe Accident Test Station (SATS) in order to optimize processing and compositional parameters for improved performance under these conditions. Failure is judged to occur when runaway oxidation is indicated by an abrupt and continuous increase in mass. Table 4 summarizes a series of failed specimens that appeared to have melted along with the conditions to which they were exposed. The resultant outer oxides of these samples were removed then ground into a fine powder using an alumina mortar and pestle.

Table 4. Alloy compositions from which outer oxides were removed to test melting behavior

Specimen #	Code	Nominal composition (wt%)	Test conditions
11597	B106Y4	Cr-10 Al-6 Y-0.04	25-1200°C in 1h - hold 1h.; 1200 to 1400°C in 1h - hold 1h; Ar purge (500cc/min) to temp. then steam (200ml/h);
11501	F5C5AY45H4	Cr-15 Al-5 Y-0.04	25-1450°C in 1h - hold 4h.; Ar purge (500cc/min); Ar off, steam on (200ml/h);
11344	B055YRH	Cr-05 Al-05 Y-0.04	25-600°C at 40°C/min then 600°C to failure (1130°C) at 5°C/min
11588	C06M3H4	Cr-10 Al-6 Mo-2 Y-0.04	25-1300°C in 1h - hold 4h.; Ar purge (500cc/min); Ar off, steam on (200ml/h);
11523	B136Y4H4	Cr-13 Al-6 Y-0.04	25-1400°C in 1h - hold 4h.; Ar purge (500cc/min); Ar off, steam on (200ml/h); Sample exploded
11584	C36M2RH	Cr-13 Al-6 Mo-2 Y-0.04	25-600°C at 40°C/min then 600°C to failure (1450°C) at 5°C/min

2.3.2 Experimental procedure

A differential scanning calorimetry (DSC) coupled thermogravimetric (TG) method with the Netzsch STA 449 F1 Jupiter was used to investigate the phase transitions in the Fe-Cr-Al-O system with the primary aim of determining the solidus of the oxides as a function of Fe, Cr, and Al composition. With DSC, both reaction temperatures and the associated enthalpy (ΔH_{rxn}) can be determined. For this work, the oxide samples were in powder form and loosely packed into a Pt-20%Rh crucibles. Since the metal

standards given in Table 2 react with or fuse to Pt and/or Rh, no sensitivity calibration was performed and therefore the ΔH_{rxn} are not quantitative.

2.3.3 Results

To validate the accuracy of the DSC/thermocouple unit, a Fe_2O_3 standard was analyzed, Figure 3. The transition temperatures for the reactions given by Eqns. 1 and 2 agree well with those determined experimentally by Muan et al. [21].

$$3Fe_2O_3(s) = 2Fe_3O_4(s) + O_2(g) \quad (1)$$

$$Fe_3O_4(s) = Fe_3O_4(l) \quad (2)$$

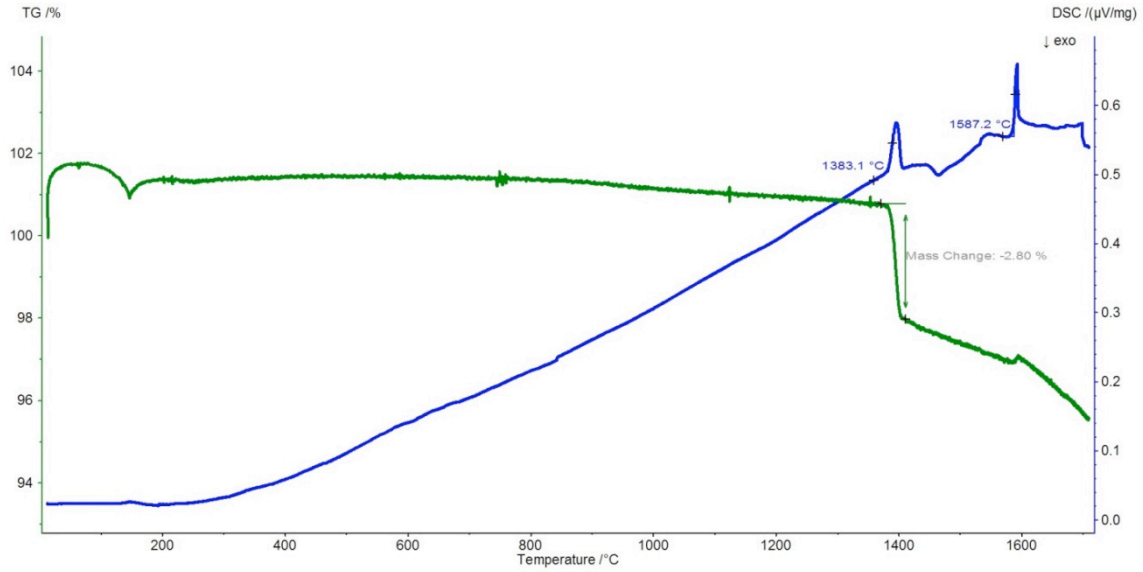

Figure 3. Recorded TG and DSC signal with temperature in an Ar-20%O_2 atmosphere for starting material Fe_2O_3 used as a standard to verify accuracy of the thermocouple for subsequent oxide studies.

The theoretical mass loss (Δm) using Eqn. 1 is 3.4%; however, a decomposition from Fe_2O_3 to hyper stoichiometric $Fe_3O_{4.14}$ as shown in Figure 4 is expected making the calculated $\Delta m = 2.4\%$ in better agreement with the experimentally observed ~2.8%. The small discrepancy between the two could lie in the fact that none of the TG measurements in this work were corrected for the buoyancy effect that arises from a dynamic temperature ramp. It also could be that the models overestimate the hyperstoichiometry of Fe_3O_4+x. This is possible since the calculated temperature for the reaction is in poor agreement with that determined experimentally in ref. [21].

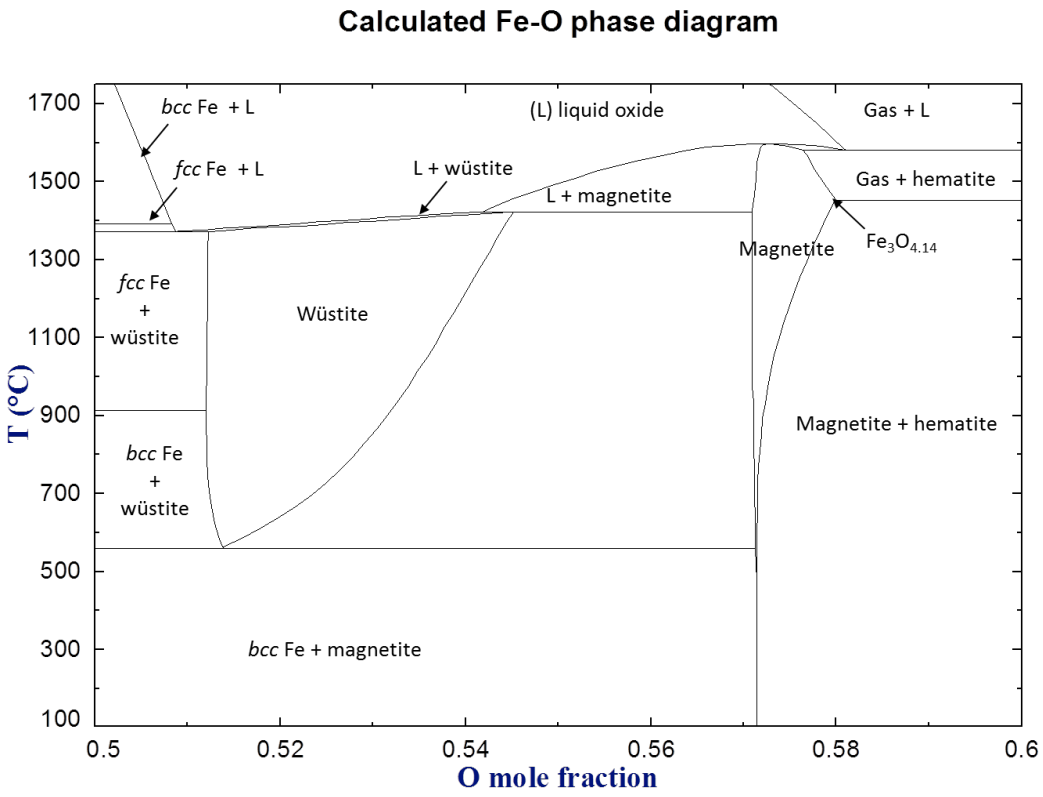

Figure 4. Calculated phase relations in a section of the Fe-O binary system using the CALPHAD models [22].

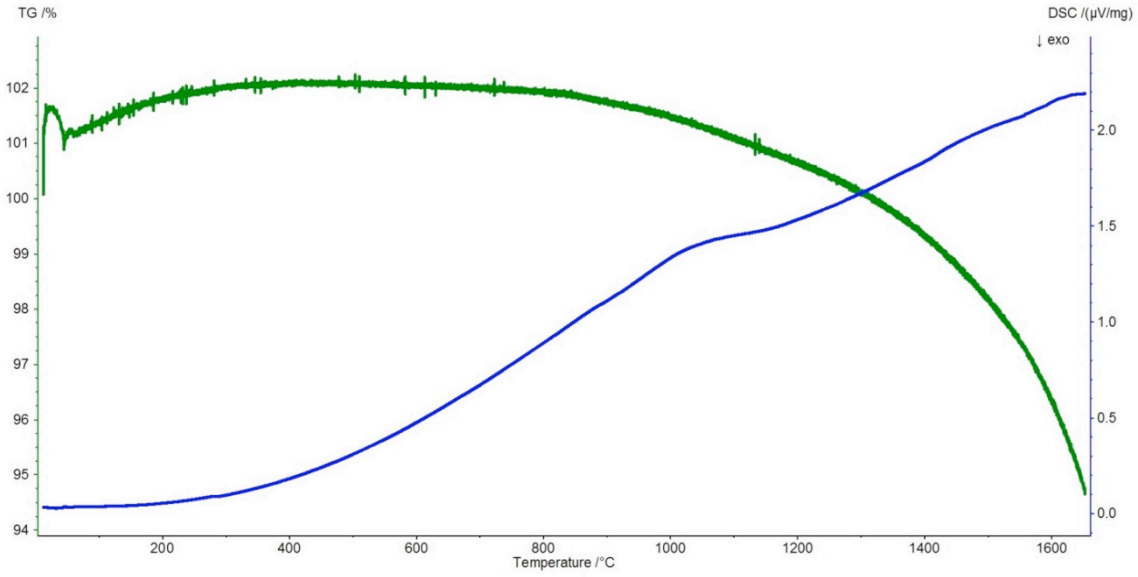

Figure 5. Recorded TG and DSC signal for sample 11597 in an UHP Ar atmosphere.

Figure 5 shows sample 11597 was most likely a spinel solution since no decomposition occurred when heated in 99.999% Ar (ultra-high purity (UHP)). This is consistent with X-ray diffraction (XRD) analysis on the oxide prior to the measurement detecting peaks for mostly a spinel $Fe_{2.67}O_4$ therefore suggesting significant dissoluiton of Al and Cr into that phase. When heated in Ar-20% O_2, the spinel $(Fe,Al,Cr)_3O_4$ solution fully oxidized at the beginning of the run to a corrundum structure $(Fe,Cr,Al)_2O_3$ and then decomposed back to the more stable spinel at 1432 °C as shown in the Figure 6. XRD of sample 11501 showed approximately half $(Fe,Al,Cr)_2O_3$ and half $(Fe,Cr,Al)_3O_4$ with some unidentified minor peaks; the contrast between XRD results for 11597 and 11501 is likely a result of the differing SATS test conditions.

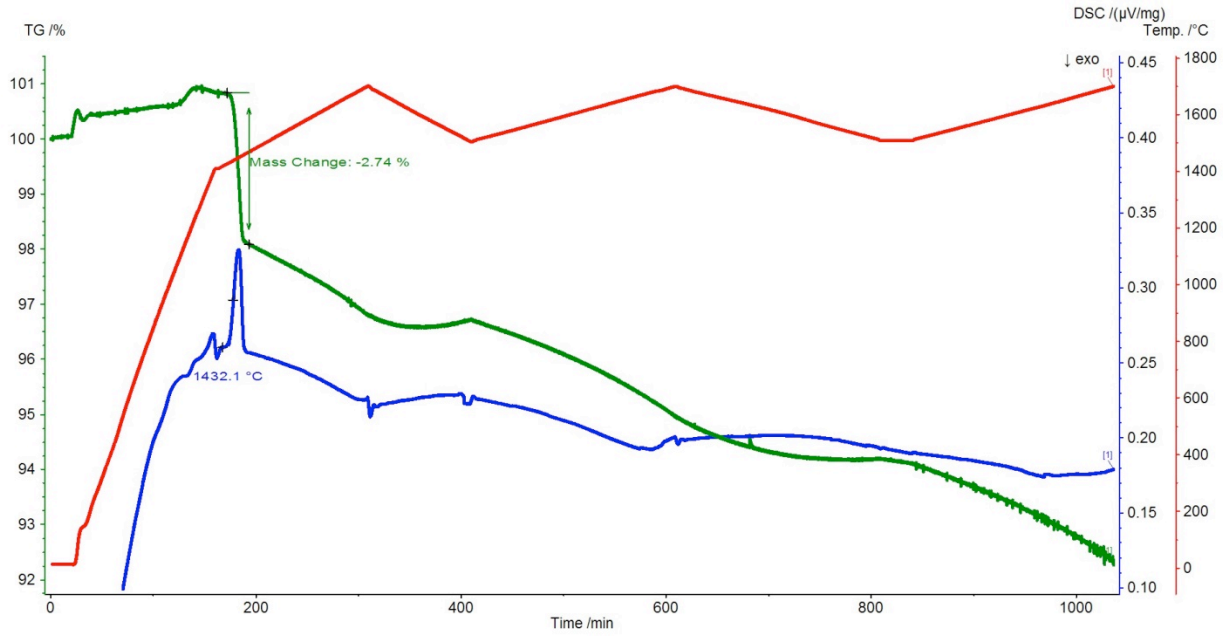

Figure 6. Recorded TG and DSC signal with temperature for the oxides of sample 11501 in an Ar-20%O_2 atmosphere.

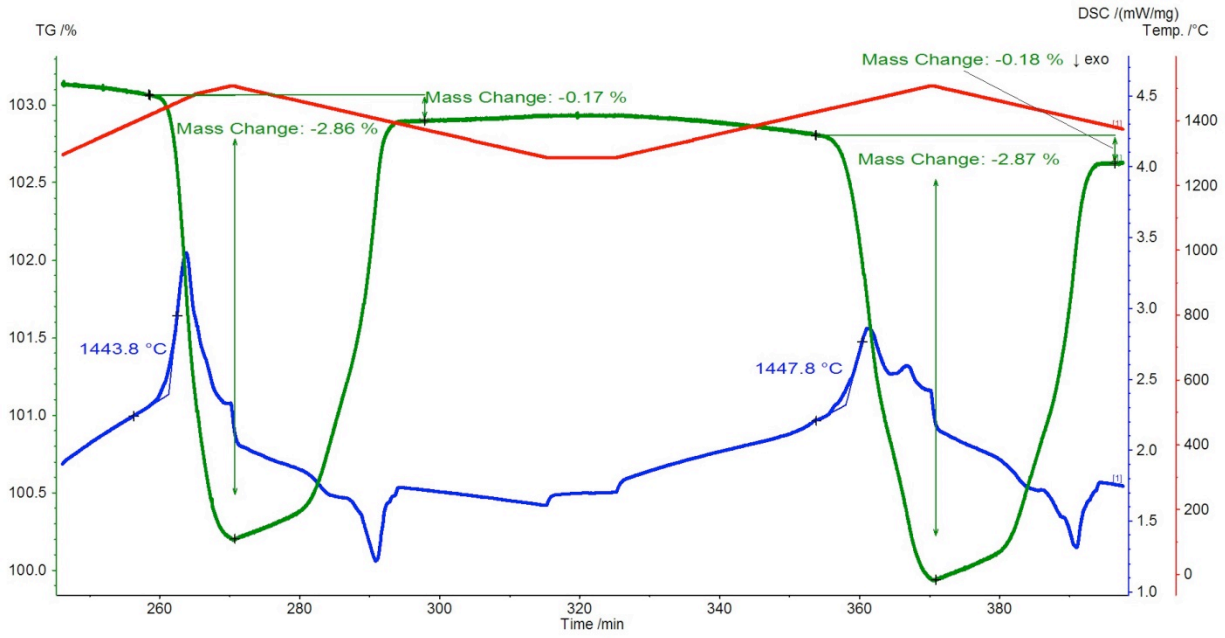

Figure 7. Recorded TG and DSC signal for sample 11597 showing cycling through the transition temperature in Ar-20% O_2 illustrating the reversibility of the reaction $3(Fe,Al,Cr)_2O_3 = 2(Fe,Al,Cr)_3O_4 + O_2$.

Figure 7 shows the reversibility of the reaction given by Eqn. 3 for sample 11597 in an Ar-20%O_2 atmosphere.

$$3(Fe,Al,Cr)_2O_3(s) = 2(Fe,Al,Cr)_3O_4(s) + O_2(g) \quad (3)$$

Excluding the corrundum-spinel transition, both Figure 6 and Figure 7 show increasing mass loss with temperature. This is due to volatilization of the oxide mainly from high vapor pressures of CrO_3 gas (p_{CrO_3}). Using thermodynamic arguments and assuming an equilibium p_{CrO_3} is maintained, given the flow rate of 100 cc/min (see note) of Ar-20% O_2, a mass loss from evovled CrO_3 (Δm_{CrO_3}) of 0.113% can be caclulated via Eqn. 4 where R is the ideal gas constant and T is absolute temperature. This is a simplistic model that agrees well with the ~0.17% observed experimentally in Figure 7. Again, the agreement could be better if the measurements were corrected for bouyancy.

$$\Delta m_{CrO_3} = \frac{p_{CrO_3} \times 1\,\text{bar} \times 100\,\text{cc/min} \times t}{RT} \quad (4)$$

A series of ceramographic analyses were performed on sample 11501 quenched by free-fall cooling from 1700°C to room temperature as shown in Figure 8. No conclusive evidence of melting could be determined. The transition temperatures for the reaction given by Eqn. 3 are summarized in Table 5.

[1] Note: Strictly speaking, the total volumetric flow rate is 100cc/min plus the CrO_3(g) contribution, but the value is insignificant and can be neglected

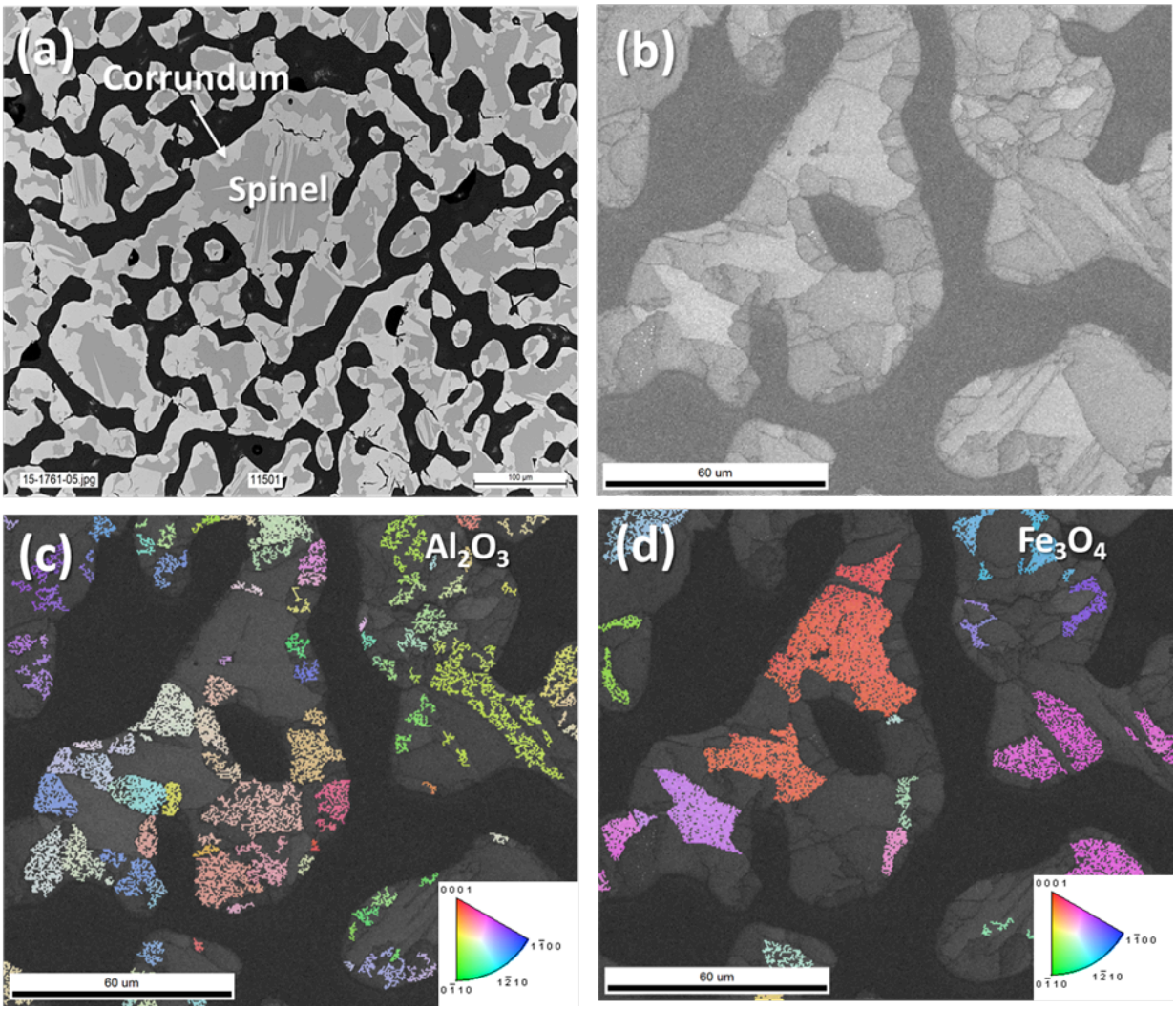

Figure 8. (a) Optical micrograph and (b) SEM image for sample 11501 quenched by freefall from 1700°C to room temperature. EBSD results for the (c) Al_2O_3 and (d) Fe_3O_4 phases respectively in the same material.

Table 5. Transition temperatures of the reaction given by Eqn. 3 for the oxides studied in this work

Specimen	$\frac{Fe}{Cr+Fe+Cr}$	$\frac{Cr}{Cr+Fe+Al}$	$\frac{Al}{Cr+Fe+Al}$	T/°C	ΔH_{rxn}/kJ·gram^{-1}
Fe_2O_3 standard	1	0	0	1383.2	530[§]
11597	0.78	0.10	0.12	1445.8	N/A
11501	0.75	0.15	0.10	1432.1	N/A
11584	0.66	0.05	0.28	1391.8	N/A
11344	0.85	0.05	0.10	1377.1	282[*]
11588	0.78	0.10	0.12	1398.4	N/A
11523	0.75	0.13	0.12	1418.5	474

[§]Calculated using the FactSage database [23] to determine the sensitivity factor for converting heat flux DSC µVs signal to mJ.
*Higher error due to overlapping temperature segments during the reaction.

2.4 CONCLUSION

The solidus temperatures for the metal alloys given in Table 3 were determined using the thermal arrest method. The oxides of failed FeCrAl specimens showed no DSC peak indicative of melting up to 1700°C. However, the free poured powders did densify significantly with sample 11501 measuring ~68% of the theoretical value; so it is possible that liquid did form. In fact, sintering temperatures were used to approximate the solidus by Muan et al. [16] for the Fe_3O_4-Fe_2O_3-Cr_2O_3 system. The change in the DSC curve from decreasing to increasing as the maximum temperature of 1700°C is approached could be the beginning of a solid-liquid phase field. However, in the absence of a clear DSC signal indicative of a phase transition, melting onset is indeterminate for the oxides and must be estimated to occur at or above 1700°C in Ar-20%O_2 atmospheres for all compositions studied. However, the results from this work do allow for a refinement of the preliminary Fe-Cr-Al and Fe-Cr-Al-O thermodynamic assessments to support further development of FeCrAl alloys as an accident tolerant replacement for Zr based cladding.

3. ANALYSIS SETUP

Several SBO severe accident simulations were performed modeling the FeCrAl ATF concept and the results for key figures of merit are compared against baseline results using the traditional urania fuel–Zr-based cladding system (see Section 4). This section describes the accident scenarios chosen, figures of merit used in the comparison, MELCOR code, plant model, and the modeling of FeCrAl in MELCOR.

3.1 FIGURES OF MERIT

Key figures of merit, provided in Table 6, were defined related to the timing of the accident progression and flammable gas generation.

Table 6. Figures of Merit Descriptions

Figure of merit		**Significance**
Timing	0.5 kg of H_2 is generated	Onset of hydrogen generation
	First fuel failure (cladding gap release)	First release of radionuclides from fuel
	100 kg of H_2 is generated	Significant combustible gas generated
	First cladding metal melting	Degradation of coolable geometry
	First cladding collapse	Degradation of coolable geometry
	Lower head failure	Escalation of accident to ex-vessel
	Containment failure	Loss of radionuclide barrier
	First deflagration in building	Escalation of accident
	0.5 kg of noble gas release to environment	Onset of radionuclide release to outside
Total mass	H_2 gas generated by 32 h	Flammable gas potential
	CO gas generated by 32 h	Flammable gas potential

Note, a figure of merit in a previous study [13] used the terminology “first cladding melting” which corresponded to the collapse of the fuel. The present report expands upon and clarifies this terminology to refer to the first melting of metallic cladding and the subsequent first collapse of the cladding. As shown in Section 4, the timing between the initial melting of the metallic cladding and collapse of cladding is quite short in general.

3.2 OVERVIEW OF TOOLS

MELCOR is a system level code that models the progression of severe accidents in light water nuclear power plants. It was developed and has been maintained by Sandia National Laboratories for the US NRC. The code encompasses various phenomena that can occur during a severe accident including the thermal-hydraulic response; the heat up, degradation and relocation of the core material; transport of radionuclides; and hydrogen generation and combustion. MELCOR is primarily used to estimate the source term from severe accidents.

Previous preliminary simulations [4] of the FeCrAl ATF concept were performed using MELCOR 1.8.5. A number of modeling improvements are included in MELCOR version 1.8.6. One key modeling change was the treatment of the reactor vessel bottom head. MELCOR version 1.8.6 [14] is still widely used internationally. From version 1.8.6 to 2.1, the major code improvements were primarily related to the code internal structure, and changes were also made to the code input structure. The updates between versions 1.8.6 and 2.1 should have limited or no impact on the simulation results of the current study. In this study, MELCOR version 1.8.6(.4073), as compiled by ORNL personnel using the Intel 11.1.064 compiler, is used on a Linux-based computer with Intel-based hardware. A few minor source code changes were required to model FeCrAl and are discussed in Section 3.4. MELCOR 1.8.6 was selected

instead of MELCOR 2.1 as the source code for MELCOR 1.8.6 was made available to incorporate the minor changes required for FeCrAl.

3.3 PLANT MODEL DESCRIPTION

The MELCOR plant model used is for Peach Bottom (Unit 2 or 3), a BWR series 4 (BWR/4) with a Mark I containment. The model includes all major components, including the reactor, containment, reactor building, various cooling systems (pumps, sprays, piping, tanks), as well as system and scenario control logic. The model has been updated from MELCOR 1.8.5 for use in MELCOR 1.8.6. This update, the model's lineage, and additional model updates have been previously described [24].

The BWR/4 with Mark I containment include a number of key systems which have interplay during a SBO accident. These are briefly summarized as follows. The reactor core isolation cooling (RCIC) system and the high pressure coolant injection (HPCI) system are steam driven pumps which can inject water into the reactor pressure vessel (RPV). Without other water injection means (from systems relying on alternating current (AC) power or alternate external systems), these systems are used during station blackout as long as direct current (DC) power remains. These systems have various trip settings, including net positive suction head limits and low steam line pressure. The safety relief valves (SRV) are valves on lines coming off of the main steam lines which can vent steam from the RPV to the suppression pool. The suppression pool (aka suppression chamber) is a large water pool located in the torus (aka wetwell) vessel near the bottom of the Mark I containment. Without access to an external ultimate heat sink (due to loss of AC power or other events), this pool serves as the heat sink to condense steam being released from the RPV. The rate of containment pressurization is slowed by condensing this steam. However, once the suppression pool becomes saturation (or near saturation conditions) the ability of the pool to condense steam is thwarted and the rate of containment pressurization increases.

Within the model, there are different competing failure modes for various structures in the system. Minor differences in the accident progression (i.e., due to material properties) may result in a different failure mode. Differences in failure modes can cause simulations to vary more substantially from one another. The following paragraphs summarize the available competing failure modes modeled for some of the components of interest.

There are three competing modes modeled for lower head failure: thermal failure of a penetration due to high temperature of a penetration or the lower head, lower head yielding via creep-rupture, and RPV over-pressurization. The over-pressurization failure mode will not occur during the accident scenarios selected. Therefore, there is a competition between failure of a penetration due to high temperature and yielding of the lower head.

There are four competing failure modes of the containment modeled. Three are functions of pressure and local temperature and include rupture of the wetwell, rupture of the drywell liner, and leakage of the drywell head flange. The final mode is the melt-through of the drywell liner due to contact by molten core materials. Each failure mode opens different release paths for radionuclides and combustible gases into the reactor building.

3.4 MODELING FeCrAl ATF CONCEPT IN MELCOR

The FeCrAl material was modeled in MELCOR by replacing the material properties for the Zr and ZrO_2 materials with those of FeCrAl and FeCrAl oxide. With this approach, the oxide, which is comprised of various species, is modeled as a single material with effective bulk properties and degradation behavior.

Recent work performed by Idaho National Laboratory, developed a separate version of MELCOR 1.8.6 that has a built in material option for FeCrAl for the cladding. However, the FeCrAl material option has not been extended to include the channel box material.

3.4.1 Thermophysical Properties

The density, thermal conductivity, specific heat and enthalpy for metallic FeCrAl, Figure 9, were modeled after Kanthal APM. The high temperature properties were linearly extrapolated to 2000 K from the available data and held constant for temperatures above 2000 K. The heat of fusion was assumed to be 275 kJ/kg.

The oxide properties are summarized in Table 7. The density is assumed to be 5180 kg/m^3 which is representative of Fe_3O_4 and is also the default MELCOR value for stainless steel oxide. The thermal conductivity is assumed to be 4.0 W/m K and is representative of Fe_3O_4. The specific heat was modeled as a function of temperature based on weight averaging of the individual Fe_3O_4, Cr_2O_3 and Al_2O_3 oxides assuming a base material composition of 82wt.%Fe-13Cr-5Al. The heat of fusion was estimated to be 664 kJ/kg based on a weight averaging of the individual Fe_3O_4, Cr_2O_3 and Al_2O_3 oxides assuming 82wt.%Fe-13Cr-5Al FeCrAl. The specific heat was modeled as 900.0 J/kg K. With respect to enthalpy, the heat of fusion was applied at melting point temperature. As discussed in Section 3.4.4, the melting temperature for the FeCrAl oxide was parametrically varied.

Table 7. Material properties for FeCrAl and FeCrAl Oxide

Assumed material properties	FeCrAl	FeCrAl Oxide
Melting point (K)	1,804	Parametrically varied 1870, 1880, 1973
Heat of fusion (J/kg)	275,000	663,867
Density (kg/m^3)	Kanthal APM (Figure 9)	5,180
Thermal conductivity (W/m K)		4.0
Specific heat (J/kg K)		900.0

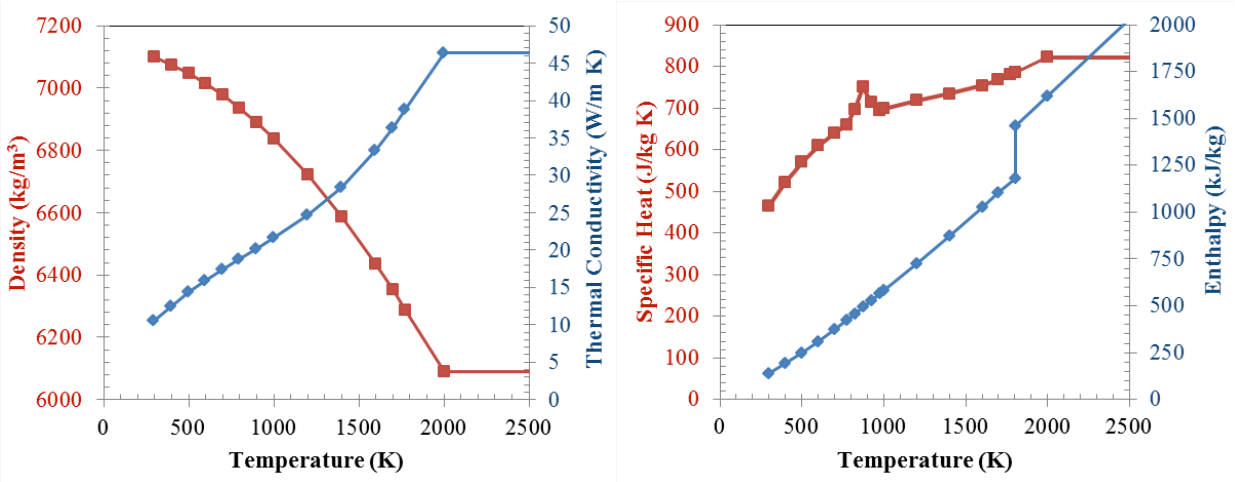

Figure 9. Modeled FeCrAl properties: density and thermal conductivity (A); specific heat and enthalpy (B).

3.4.2 Oxidation

The oxidation kinetics of FeCrAl with steam while in vessel was modeled by Eqn. (5, 6) where K(T) is the oxidation rate constant based on the mass of metal consumed during oxidation, and T is temperature in Kelvin.

For temperatures less than 1773 K (1500°C), the aluminum in the FeCrAl oxidizes to form a protective scale limiting further corrosion. Therefore, the oxidation rate equation for temperatures less than 1773 K (1500°C) is based on the oxidation of Aluminum into Al_2O_3. The parabolic rate equation, for the mass of metal oxidized, is given by Eqn. (1) and is based on experimental data reported for FeCrAl from ref. [25].

For temperatures 1773 K (1500°C) and above, the protective Al_2O_3 scale fails and oxidation of the iron proceeds rapidly. Therefore, the oxidation kinetics of FeCrAl, at 1773 K (1500°C) and above, is based on 304 stainless steel which is dominated by the oxidation of iron. The parabolic rate equation, for the mass of metal oxidized, is given by Eqn. (2) and is based on the default values used by MELCOR for the oxidation of stainless steel [14].

$$K(T)=\left(230.0\ \frac{kg^2 metal}{m^4\ s}\right)\cdot \exp\left(\frac{-41376.0\ K}{T}\right) \qquad T<1773\ K \tag{5}$$

$$K(T)=\left(2.42x10^9\ \frac{kg^2 metal}{m^4\ s}\right)\cdot \exp\left(\frac{-42400\ K}{T}\right) \qquad T\geq 1773\ K \tag{6}$$

The oxidation kinetics of FeCrAl with oxygen while in vessel were based on the kinetics of Zircaloy reaction with oxygen but reduced by three orders of magnitude. However, the reaction of FeCrAl with O_2 while in-vessel has limited importance during in-vessel core degradation for the accident scenarios chosen.

The heat of oxidation for zirconium- and steel-based materials is hardcoded in MELCOR. To more accurately reflect the FeCrAl material, the heat of oxidation for reaction of FeCrAl with H_2O and O_2 was modified in the MELCOR source code. The modification was performed to reflect FeCrAl comprised of 73wt.%Fe-22Cr-5Al with production of Fe_3O_4, Cr_2O_3 and Al_2O_3 oxides. The heat of reaction (at 298 K) for FeCrAl was taken to be 1.247 MJ/kg for reaction with H_2O, and 8.837 MJ/kg for reaction with O_2. Note, a more representative alloy composition for reactor application, 82wt.%Fe-13Cr-5Al, has lower heat of reactions of 0.9897 MJ/kg with H_2O and 8.451 MJ/kg with O_2.

The oxidation reaction equation for MELCOR's Zr material was modified to reflect the stoichiometry of oxidizing 73wt.%Fe-22Cr-5Al FeCrAl. The FeCrAl cladding emissivity, as a function of oxide thickness, was modeled the same as the default in MELCOR for Zircaloy. However, the maximum emissivity of oxidized cladding was set to 0.70.

3.4.3 Fuel and Cladding Geometry

The cladding thickness was reduced by 50% while maintaining the cladding outer diameter. This resulted in 43% less cladding material mass than in the base case. The channel box dimensions remained constant. The gap between the fuel pellet and cladding was assumed to be zero in both the UO_2-FeCrAl and UO_2-Zircaloy models. The fuel pellet outer diameter was increased to offset the reduction in cladding thickness. This resulted in the UO_2 mass increasing by 18.5%. The reduction in cladding thickness is based on previous reactor physics assessments of FeCrAl cladding in PWRs in which it was determined that maintaining operational cycle lengths was best accomplished through a small increase in batch-average enrichment and reduction of the cladding thickness to about half of the nominal thickness [10, 26, 27]. Recent neutronics studies found similar results for BWRs as well; however, the studies suggest reducing both the cladding and channel box thicknesses by about 50% [28, 29]. Reducing the channel box thickness impacts core thermal hydraulics with respect to flow area. Modeling a reduced channel box thickness is left for future work.

3.4.4 Fuel Degradation and Relocation Characteristics

For Zircaloy cladding, there are numerous tests on its behavior under accident conditions [30]. Testing covers the heat up, burst, oxidation, melting, and relocation of the cladding. MELCOR simulates the burst of the rods and models oxidation of the cladding, buildup of oxide thickness, and the melting/candling of the metallic Zircaloy. As modeled in MELCOR, the melting point of Zircaloy is 2098 K (1825°C) and zirconium oxide is 2990 K (2717°C). Based on test observations, the oxidized cladding can remain standing while molten metallic Zircaloy relocates. Based on PHEBUS tests, the point at which oxidized cladding is assumed to fail and relocate downwards is 2500 K (2227°C). Many of these melting and relocation temperatures are able to be modified by the MELCOR user.

Failure and relocation of a FeCrAl clad fuel rod, under accident conditions, still remains to be experimentally investigated. The melting point of the metallic FeCrAl was modeled as 1804 K (1531°C) based on computed values that were experimentally verified at ORNL, see Section 2.2.3. The melting point, or effective melting point of the oxide structure was also investigated at ORNL, see Section 2.3.3. There was not clear evidence of oxide melting, up to the 1973 K (1700°C) conditions tested. The melting point of the individual oxides, Al_2O_3 or Cr_2O_3, is quite high, over 2273 K (2000°C). However, the melting point of Fe_3O_4 (approximately 1597°C) [14], FeO (approximately 1377°C), and decomposition temperature of Fe_2O_3 (approximately 1,539–1,565°C) is quite low compared to zirconium oxide. Above some temperature, modeled as 1773 K (1500°C) for the oxidation kinetics (Section 3.4.2), the protective Al_2O_3 scale fails and there is continued and rapid oxidation of the iron. Unlike the ZrO_2 oxide, which can remain structurally intact for some time, the iron oxide is unlikely to remain in a rod like geometry. Given the uncertainty in the temperatures at which the FeCrAl oxide melts and at which FeCrAl clad will fail and relocate downwards, a range of temperatures were assumed and are discussed in Section 3.5.2. The effective melting and failure temperature, for the FeCrAl cladding oxide under prototypic accident conditions, requires further research.

The formation of eutectics greatly influences the core degradation process in the existing reactors utilizing Zircaloy [16]. Note that B_4C and steel, relevant for the control blades, have a eutectic modeled as 1420 K (1147°C) in MELCOR. Bechta, et. al. found a eutectic between FeO and UO_2 at 1610 K (1337°C) [31]. In discussion of the PHEBUS tests [32], it was noted the potential for FeO_x to interact with UO_2. Previous separate effects tests using a UO_2 crucible loaded with FeO powder, experience rapid penetration of the FeO into the UO_2 under the 1673 K (1400°C) inert atmosphere test conditions [33]. The potential eutectic formation of FeCrAl with B_4C, Inconel, and UO_2 was not modeled and needs to be investigated in the future.

For Zircaloy, another failure mode is modeled for the cladding. Once the cladding exceeds 2400 K, a time-at-temperature criterion for cladding failure is activated. The cladding is modeled to remain intact only for a specified amount of time depending on the temperature. This is included in the model to preclude very hot, or once very hot, cladding from standing indefinitely. This type of data is not available for FeCrAl cladding. The time-at-temperature criterion was kept for FeCrAl; however, it will not be activated due to the high temperature (2400 K) required.

3.4.5 Radionuclide Inventory and Decay Heat

The core radionuclide inventory and distribution and the total decay heat and distribution were not modified and were the same as the model with zirconium clad fuel. To date, a reference assembly design has not been developed that can accommodate the integral considerations of thermal-hydraulics, neutronics, fuel performance, and economics. Once a FeCrAl ATF fuel assembly design is developed, the radionuclide and decay heat distributions should be revised.

For both Zircaloy and FeCrAl cladding, the rods are assumed to burst and release their radionuclides residing in the gap at 900°C. In reality, the rod burst phenomenon is both function of rod pressure and temperature. The burst characteristics of 1st generation FeCrAl alloy claddings have been investigated [34]. For the same hoop stress, the FeCrAl clad was shown to have improved burst

characteristic, ~10% higher burst onset temperature. The FeCrAl cladding was also shown to have different ballooning characteristics, i.e. lower strain.

3.4.6 Note on Ex-Vessel Modeling

The core-concrete interaction modeling in MELCOR is performed by a separate package (based on CORCON-Mod3) with its own material properties. During transfer of melt from in-vessel to ex-vessel, the model was modified to map the Zr and Zr oxide materials (modified to model FeCrAl) to stainless steel and stainless steel oxide materials. Thus, the FeCrAl material is treated as stainless steel by the core-concrete interaction modeling. Some insight into the consequences of this can be found in ref. [9]. Substituting stainless steel (or Zr) for FeCrAl in the ex-vessel modeling could impact the oxidation rate of the material; however, the oxidation rate is generally limited by the availability of concrete decomposition gases. The substitution impacts the amount of energy generated during oxidation, as well as the amount of hydrogen generated. The substitution will also impact the material properties predicted for the debris. This limitation could be explored and addressed in the future, but it is likely overshadowed by the limited ex-vessel debris coolability models that are integrated into the released MELCOR 1.8.6 and early 2.1 versions [35, 36].

3.5 ACCIDENT SCENARIO AND CASES

3.5.1 Station Blackout Accident Scenarios Modeled

The SBO severe accident scenario was chosen for investigation. The SBO scenario was chosen due to its high contribution to the overall core damage frequency for BWRs [37, 38]. In addition, the accidents which occurred at Fukushima Daiichi Units 1–3 were variants of the SBO scenarios [39, 40].

During the SBO scenario, the reactor is assumed to successfully trip (reference time 0 h). All AC power, including off-site and on-site power (diesel generators), is assumed to be lost at 0 h. The timing of the loss of DC power (batteries) was modeled to occur at 0 h (short-term SBO) and at 8 h, 16 h, or 24 h (long-term SBO).

While DC power is maintained, the RCIC and HPCI systems can be used to inject cooling water into the primary system. As modeled, operators do not control the speed of the RCIC or HPCI systems. Thus, they turn full-on and off as necessitated by the water level. Also, as modeled, these systems are aligned to take suction from the condensate storage tank. There are a number of trip and system isolation conditions. Pertinent to the scenarios analyzed, these systems are isolated if the main steam line pressure drops below a specified value.

While RCIC and HPCI operate, the safety relief valves (SRV) actuate automatically at their pressure set point. Manual operation of the SRVs relies on DC power and plant air availability. As modeled, the operators will manually depressurize the RPV, using the SRVs, if the suppression pool exceeds its heat capacity limit. Once DC power is lost, the ability to manually actuate the SRVs is lost, and the RPV can repressurize up to the pressure set point for automatic SRV actuation. Note, operator action to depressurize the reactor can cause isolation of the RCIC and HPCI (ceasing water injection) due to low steam line pressure.

After inject water ceases, the reactor pressure vessel water inventory boils away, uncovering the core. The fuel rods heat up, oxidize, generating heat and hydrogen, and begin fail. The failed fuel relocates downward and may eventually fail the lower head of the RPV. This core debris may interact with the concrete containment floor, oxidizing metallic species in the debris. Throughout these events, the generation of steam and non-condensable gases cause the containment to pressurize. As modeled during the scenarios, the operators do not take action to vent containment. Eventually, the containment fails releasing radionuclides and hydrogen into the reactor building. Deflagrations can occur in the reactor building and ultimately radionuclides can be released into the environment.

Three different water injection recovery scenarios were considered. In one scenario, water injection into the primary system is not restored (unmitigated SBO). In the second scenario, water injection is restored, for a specified time period, into a feedwater line at a rate of 0.454 m^3/min. After this period, the water injection is assumed to be lost for the remainder of the simulation. For the third scenario, water injection is restored indefinitely into a feedwater line at a rate of 0.568 m^3/min (150 GPM) at a specified time after the loss of DC power (mitigated SBO).

3.5.2 Melting and Failure Point Parametric Study Cases

Based on the results of Section 2.2, the melt point of the metallic FeCrAl is modeled as 1804 K.

As discussed in Section 2.3 and 3.4.4, there is uncertainty in the temperatures at which oxidized FeCrAl cladding will fail and melt. Therefore, for this work, three different FeCrAl cases are considered. Table 8 summarizes the melting and failure properties for the Zircaloy system, the three cases for FeCrAl considered in this study, and the FeCrAl case considered in a previous study [13].

Two oxide failure modes modeled are noted. The first one is the temperature at which an oxide shell is no longer able to hold up metallic melt. Above this temperature, any metallic melt will begin candling downwards. The second mode refers to the temperature up to which an oxidized cladding will remain standing if no intact metallic metal is present.

For the first FeCrAl case, the oxidized cladding is assumed to fail at the onset of rapid oxidation (1773 K). The oxide melting point is assumed to be 1870 K, which is the melting point of Fe_3O_4.
For the second FeCrAl case, the oxidized cladding is assumed to fail at 1870 K, the melting temperature for Fe_3O_4. The melting point of the oxide is then assumed to be 1880 K, 10 degrees higher than the relocation temperature. The slightly higher melting point was chosen to aid in numerical stability. Also, the FeCrAl oxide includes chromium and aluminum oxides with melting temperatures greater than 2200 K.

For the third FeCrAl case, the oxidized cladding is assumed to melt at 1973 K (1700°C). This is based on the observations of the oxide melt testing, Section 2.3. The results suggest the oxide may not melt at temperatures up to 1700 C or higher. The oxide was assumed to fail at 1963 K, 10 K below the modeled melting point.

For comparison, in the previous study [13], the metallic FeCrAl was assumed to melt at 1773 K and the oxide was assumed to melt at 1901 K. The refined value used in this study is 31 K higher than the value previously used. With respect to failure, the oxide was modeled to no longer support a metallic melt above 1773 K and could stay standing until the modeled oxide melting point, 1901 K, if no metallic melt was present. For the current study, the parametrically varied FeCrAl cases for oxide failure and melting encompass the previously used values.

Table 8. Summary of Melting and Relocation Temperatures

Cladding Case	Metal Melting & Relocation (K)	Oxide Failure		Oxide Melting (K)
		Shell Melt Hold-up (K)	Collapse* (K)	
Zircaloy	2098	2400	2800**	2990
FeCrAl Case 1	1804	1773	1773	1870
FeCrAl Case 2	1804	1870	1870	1880
FeCrAl Case 3	1804	1963	1963	1973
FeCrAl Prev. Study [13]	1773	1773	1901	1901

**The simulations used the recommended default from MELCOR 1.8.5, 2800 K. In MELCOR 1.8.6 the recommended default was revised to 2500 K. However, there is also a time-at-temperature failure mode which is activated at 2400 K. In all the Zircaloy simulations, the cladding collapses at temperatures below 2500 K.

3.5.3 Simulation Summary

The simulations analyzed in Section 4 are summarized in Table 9. In total, seven SBO scenarios are considered. For each scenario a Zircaloy base case is simulated as well as at least one FeCrAl case. As will be seen in Section 4, the FeCrAl Case 1 and Case 2 are quite similar. Therefore only FeCrAl Case 2 was simulated for accident scenarios 3-7.

Table 9. Summary of Scenarios

Scenario Type	Accident Scenario	Report Section	Timing of DC Power Loss (h)	External Water Injection		Simulation End Time (h)	Cladding Case (see Table 8)
				Timing (h)	Rate (lpm)		
Unmitigated SBO	**1**	**4.1**	0	never	NA	32	Zircaloy
							FeCrAl Case 1
							FeCrAl Case 2
							FeCrAl Case 3
							FeCrAl Prev. Study
	2	**4.2**	8	never	NA	32	Zircaloy
							FeCrAl Case 1
							FeCrAl Case 2
							FeCrAl Case 3
							FeCrAl Prev. Study
	3	**4.3**	16	never	NA	32	Zircaloy
							FeCrAl Case 2
Delayed SBO with Mitigation Failure	**4**	**4.4**	16	5 - 16	454	48	Zircaloy
							FeCrAl Case 2
	5	**4.5**	24	5 - 24	454	42	Zircaloy
							FeCrAl Case 2
Mitigated SBO	**6**	**4.6**	0	2 – end of simul.	568	32	Zircaloy
							FeCrAl Case 2
	7	**4.7**	8	16 – end of simul.	568	32	Zircaloy
							FeCrAl Case 2

NA: not applicable

4. ANALYSIS RESULTS

Sections 4.1-4.7 provide and discuss the simulation results for each scenario. Key results and takeaways are summarized in Section 4.8

4.1 UNMITIGATED STSBO

The figures of merit results for the cases are summarized in Table 10. Figure 10 through Figure 15 depict the reactor and containment pressure, RPV water level, peak intact cladding temperature, total and in-vessel hydrogen generation, fraction of cladding collapsed, and the fraction of noble gas released.

During the unmitigated STSBO, there are no operator actions or water injection by the RCIC, HPCI, or external means. Without operator actuation of the SRVs or the HPCI operating, the RPV remains pressurized until the RPV lower head fails. The RPV water level continuously drops while the water boils away. The lower head dries out faster in the FeCrAl cases than the Zircaloy case. This is likely due to the timing of debris relocation to the lower head, which is affected by the cladding thermophysical properties and oxidation kinetics. The RPV lower head fails sooner for the FeCrAl cases than for the Zircaloy case. The failure of the RPV and subsequent core debris-concrete interaction results in failure of the containments. Soon after containment failure, deflagrations are predicted to occur in containment and noble gases (and other radioactive fission products) are released to the environment. The outer ring of FeCrAl assemblies is predicted to remain standing for an extended period; however, they eventually fail and relocate downwards.

When comparing the figures of merit, Table 10, of FeCrAl Case 1, 2, or 3 to the base case Zircaloy system, the onset of hydrogen generation is delayed 39 minutes. The timing to first release of the radionuclides in the gap is delayed only 4 minutes. The generation of substantial quantities of hydrogen (taken as 100 kg) is delayed by 84 minutes. The timing to initial melting of the metallic cladding is delayed 75 minutes and the initial collapse of a cladding segment is delayed 75 (Case 1), 79 (Case 2), and 91 (Case 3) minutes. After the onset of fuel damage, the FeCrAl cases exhibit a more rapid lower head failure, containment failure, and occurrence of deflagrations in the reactor building. All the FeCrAl cases produce slightly less hydrogen and carbon monoxide by 32 hours.

In general, FeCrAl Case 1, Case 2, and Case 3 progress at similar rates. Case 3, with the highest oxide melting and failure temperatures performs the best. Included in Table 10 is a previously analyzed FeCrAl case. Compared to the previously analyzed FeCrAl case, FeCrAl Cases 1, 2, and 3 exhibit less gain over the existing Zircaloy system with respect to timing or hydrogen gas generation. Recall that the previously analyzed FeCrAl case used slower oxidation kinetics above 1773 K (1500°C).

Table 10. Figure of Merit Results for Unmitigated Short Term Station Blackout

Figure of merit	Zirc.	FeCrAl Case 1	FeCrAl Case 2	FeCrAl Case 3	*FeCrAl Prev. [13]*
0.5 kg of H_2 is generated[a]	70	109	109	109	*109*
First fuel failure (gap release)[a]	72	76	76	76	*76*
100 kg of H_2 is generated[a]	97	181	181	181	*182*
First cladding metal melting[a]	112	187	187	187	*193*
First cladding collapse[a]	112	187	191	203	*223*
Lower head failure[a]	568	515	506	553	*553*
Containment failure[a]	582	541	532	569	*628*
First deflagration in building[a]	582	541	532	570	*629*
0.5 kg noble gas release to environment[a]	571	542	532	570	*629*
H_2 gas generated by 32 h[b]	3,164	3,070	2,941	2,808	*1,738*
CO gas generated by 32 h[b]	40,048	37,011	36,291	35,658	*40,858*

[a] = minute ***[b] = kg***

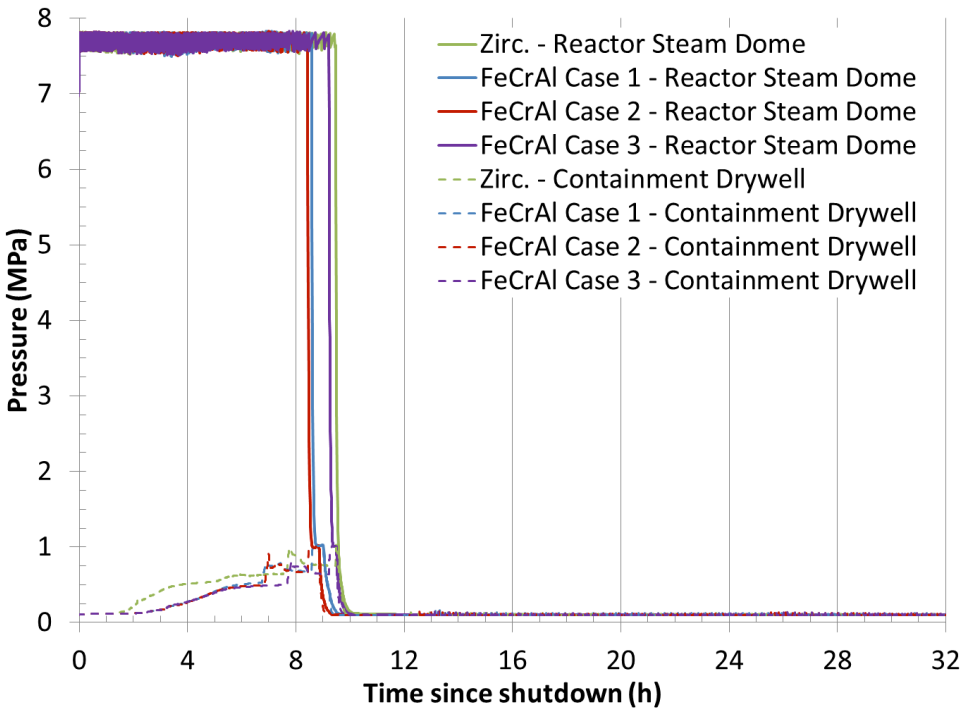

Figure 10. STSBO - Reactor and Drywell Pressure

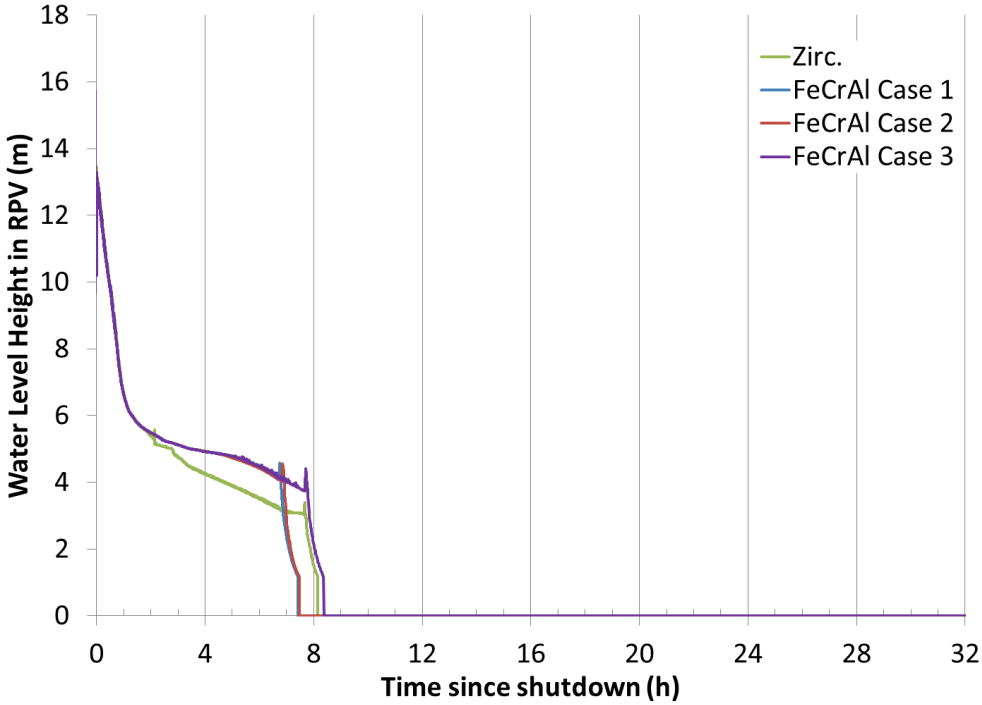

Figure 11. STSBO - RPV Water Level

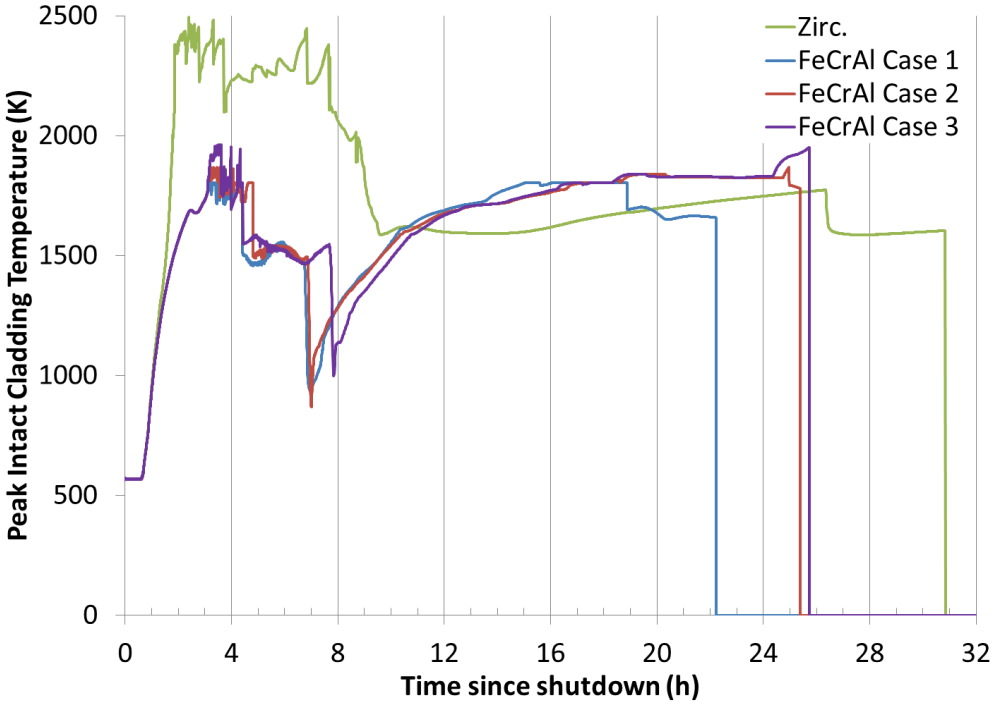

Figure 12. STSBO - Peak Intact Cladding Temperature

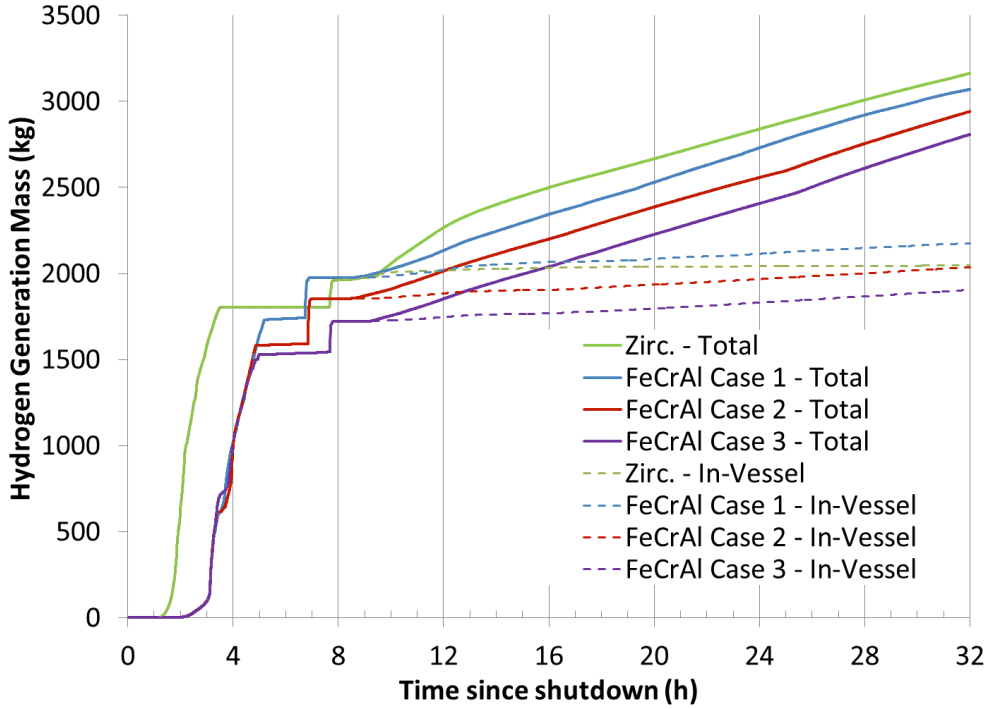

Figure 13. STSBO - Total and In-Vessel Hydrogen Generation

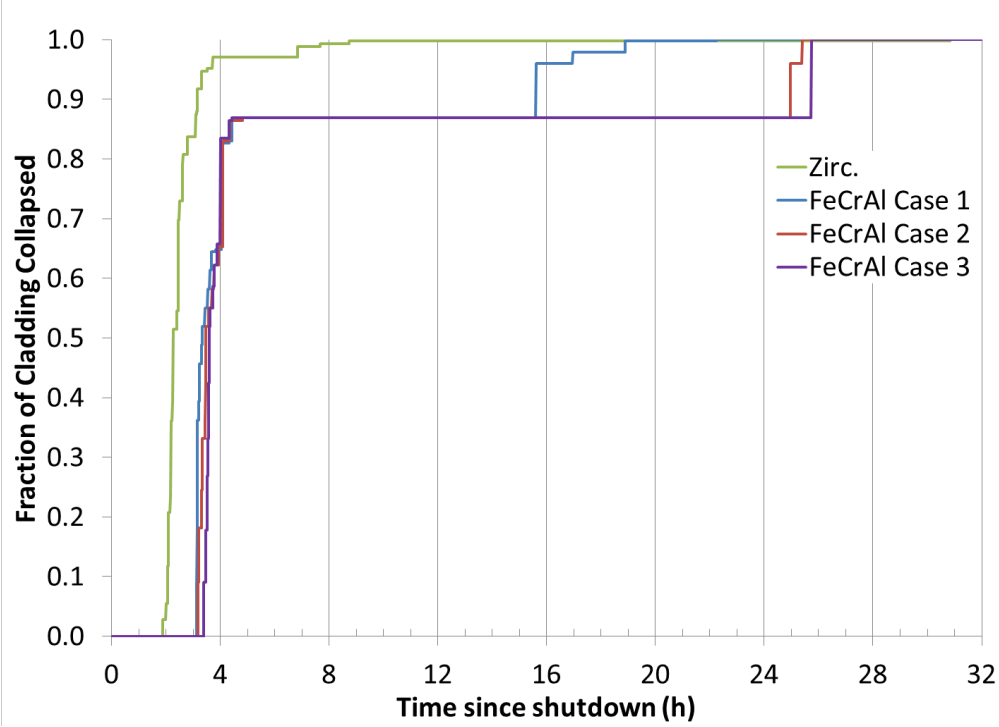

Figure 14. STSBO - Fraction of Cladding Collapsed

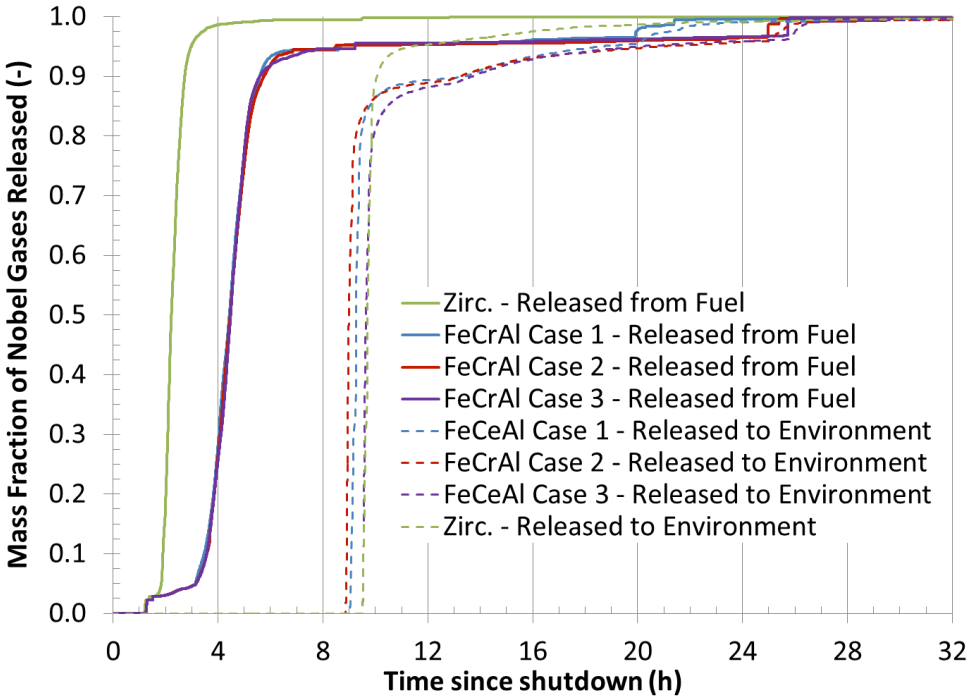

Figure 15. STSBO - Fraction of Nobel Gases Released

4.2 UNMITIGATED LTSBO WITH DC LOSS AT 8H

The figures of merit results for the cases are summarized in Table 11. Figure 16 through Figure 21 depict the reactor and containment pressure, RPV water level, peak intact cladding temperature, total and in-vessel hydrogen generation, fraction of cladding collapsed, and the fraction of noble gas released.

During this unmitigated LTSBO, the operators have DC power for 8 hours. As modeled, the operators depressurize the RPV at 2.9 hours by manually actuating a SRV due to high temperatures in the suppression chamber. The RCIC or HPCI operate until 4.4 hours when they are isolated due to low steam pressure. After cessation of water injection, the RPV water level continuously drops while the water boils away. At 8 hours, DC power is lost, the manually controlled SRV closes, and the RPV repressurizes up to the lowest automatic set point of the SRVs. As the RPV repressurizes, the water level briefly swells and then resumes boiling away. Eventually, the fuel become uncovered and begins to heat up. The Zircaloy cladding heats up faster than the FeCrAl cladding due to the oxidation kinetics. Despite its higher failure temperature, the Zircaloy cladding begins to relocate much sooner than the FeCrAl cladding. The containment is predicted to fail earlier in the Zircaloy case than in the FeCrAl cases. The earlier hydrogen generation and heat generated during oxidation of the Zircaloy contributes to the earlier pressurization and failure of containment. Soon after containment failure, deflagrations are predicted to occur in containment and noble gases (and other radioactive fission products) are released to the environment. The core debris relocates downward, eventually into the RPV lower head. The lower head dries out and fails faster in the Zircaloy case than in the FeCrAl cases. The melt relocates to the drywell where core debris-concrete interaction is predicted to occur.

When comparing the figures of merit, Table 11, of FeCrAl Case 1, 2, or 3 to the base case Zircaloy system, the onset of hydrogen generation is delayed 69 minutes. The timing to first release of the radionuclides in the gap is delayed only 8 minutes. The generation of substantial quantities of hydrogen (taken as 100 kg) is delayed by 188 minutes. The timing to initial melting of the metallic cladding is delayed 177-178 minutes and the initial collapse of a cladding segment is delayed 177 (Case 1), 183 (Case 2), and 208 (Case 3) minutes.

After the onset of fuel damage, containment failure and the onset of deflagrations in the building are delayed 89 minutes (Case 1), 152 minutes (Case2), and 146 minutes (case 3). The failure of the containment is due to the inability to manually vent containment. The release of radionuclides is delayed 88 minutes (Case 1), 151 minutes (Case 2), and 146 (Case 3) minutes. Failure of the lower head occurs late and delayed 63 (Case 1), 94 minutes (Case 2), and 112 (Case 3) minutes. All FeCrAl cases produce less hydrogen (i.e. 19% less for Case 1, 26% less for Case 2, and 21% less for Case 3) and carbon monoxide (i.e. 61% less for Case 1 and Case 2 and 65% less for Case 3) by 32 hours.

Consistent with the unmitigated STSBO, FeCrAl Cases 1, 2 and 3 progress at similar rates.

Table 11. Figure of Merit Results for Unmitigated Long Term Station Blackout – 8h

Figure of merit	**Zirc.**	**FeCrAl Case 1**	**FeCrAl Case 2**	**FeCrAl Case 3**	***FeCrAl Prev. [13]***
0.5 kg of H_2 is generated[a]	740	809	809	809	*811*
First fuel failure (gap release)[a]	746	754	754	754	*755*
100 kg of H_2 is generated[a]	791	979	979	979	*980*
First cladding metal melting[a]	827	1,004	1,004	1,005	*1,015*
First cladding collapse[a]	827	1,004	1,010	1,035	*1,034*
Lower head failure[a]	1,387	1,450	1,481	1,499	*1,512*
Containment failure[a]	1,250	1,339	1,402	1,396	*1,515*
First deflagration in building[a]	1,250	1,339	1,402	1,396	*1,525*
0.5 kg noble gas release to environment[a]	1,251	1,339	1,402	1,397	*1,516*
H_2 gas generated by 32 h[b]	2,911	2,372	2,156	2,309	*844*
CO gas generated by 32 h[b]	18,488	7,260	7,203	6,397	*6,841*

[a] = minute ***[b] = kg***

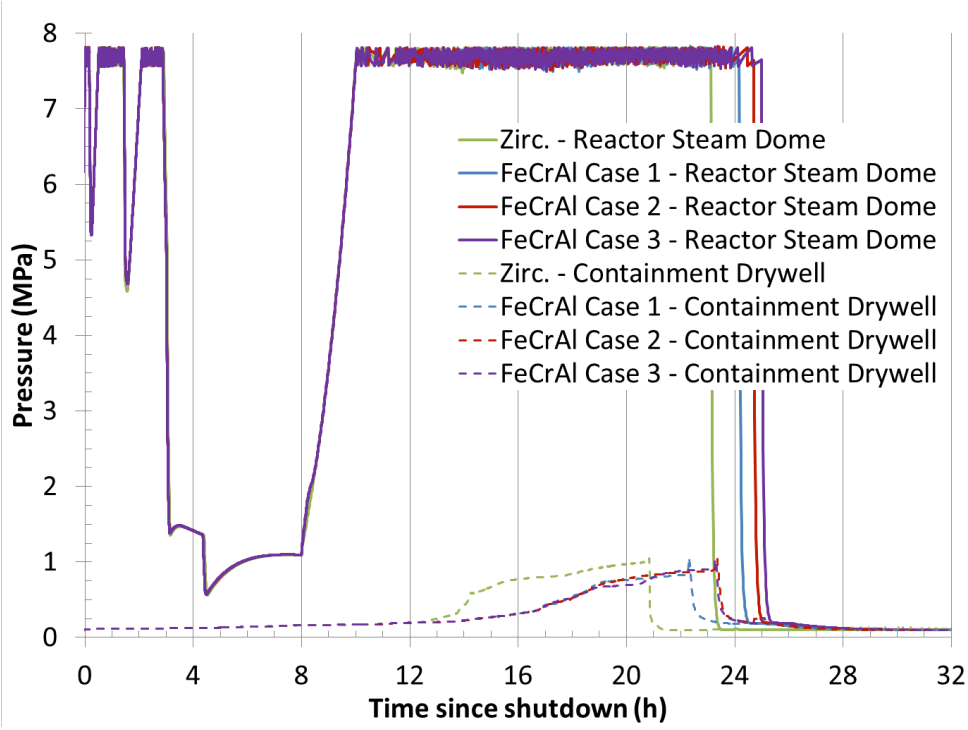

Figure 16. LTSBO 8h DC Loss - Reactor and Drywell Pressure

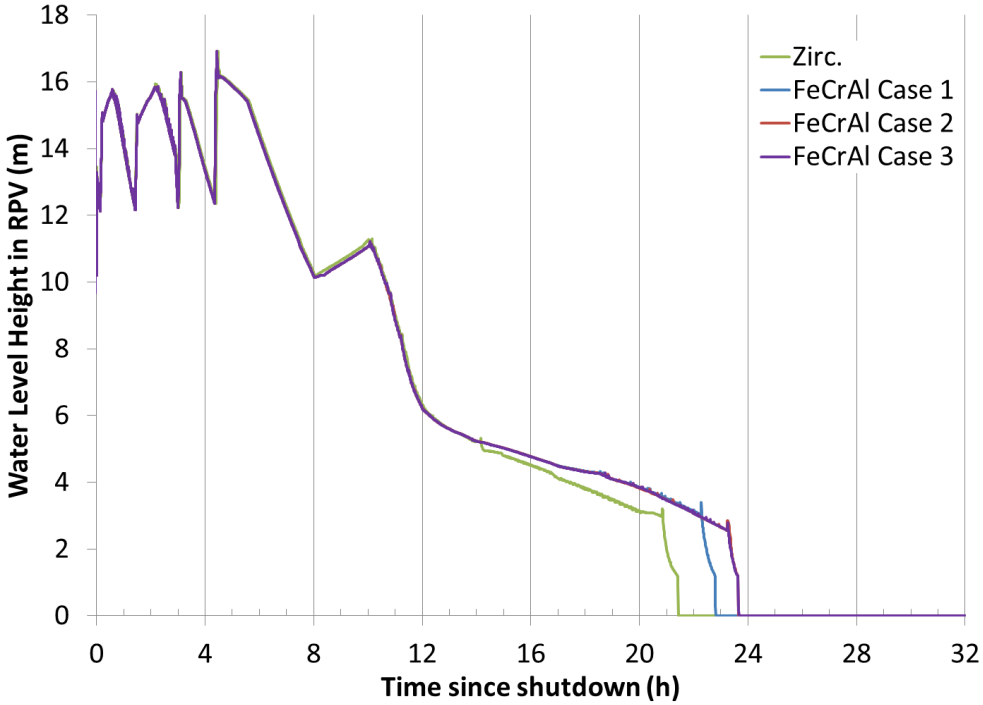

Figure 17. LTSBO 8h DC Loss - RPV Water Level

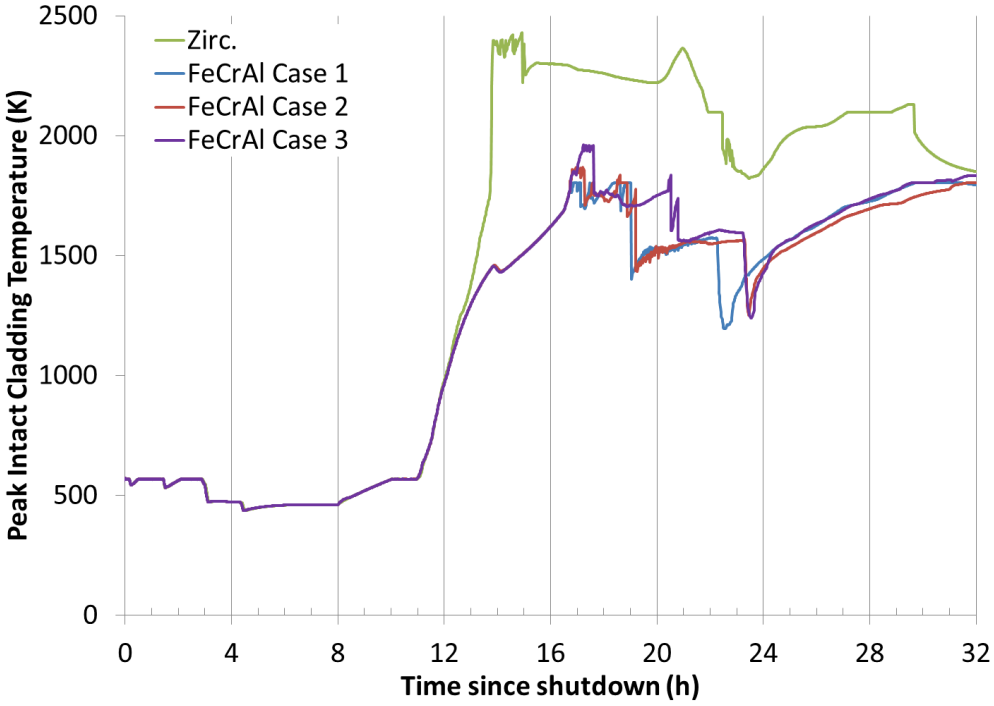

Figure 18. LTSBO 8h DC Loss - Peak Intact Cladding Temperature

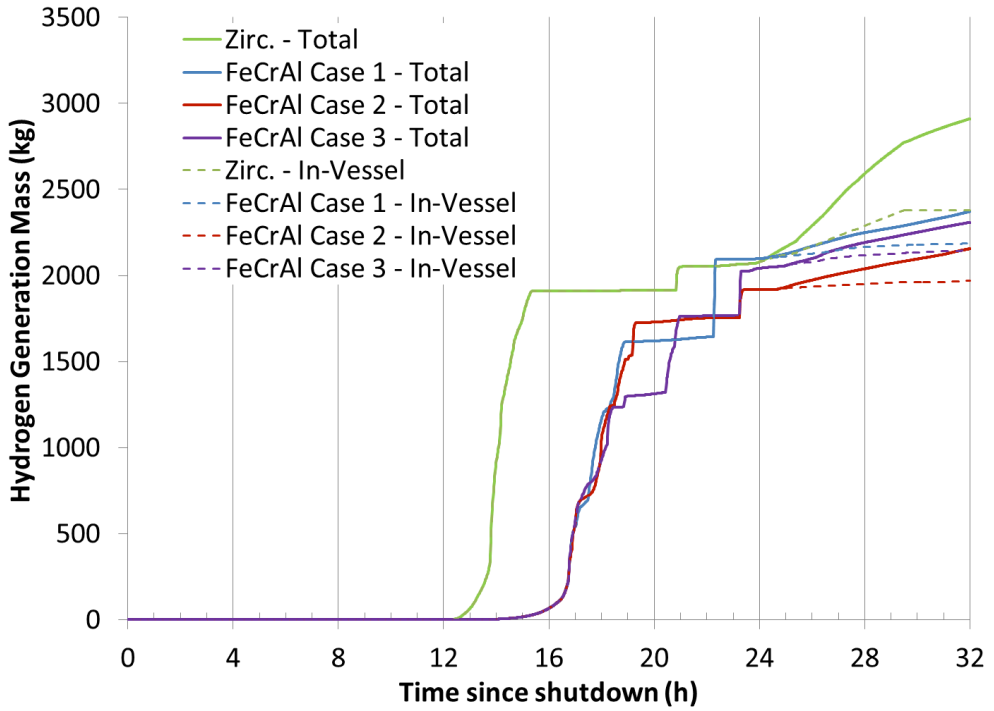

Figure 19. LTSBO 8h DC Loss - Total and In-Vessel Hydrogen Generation

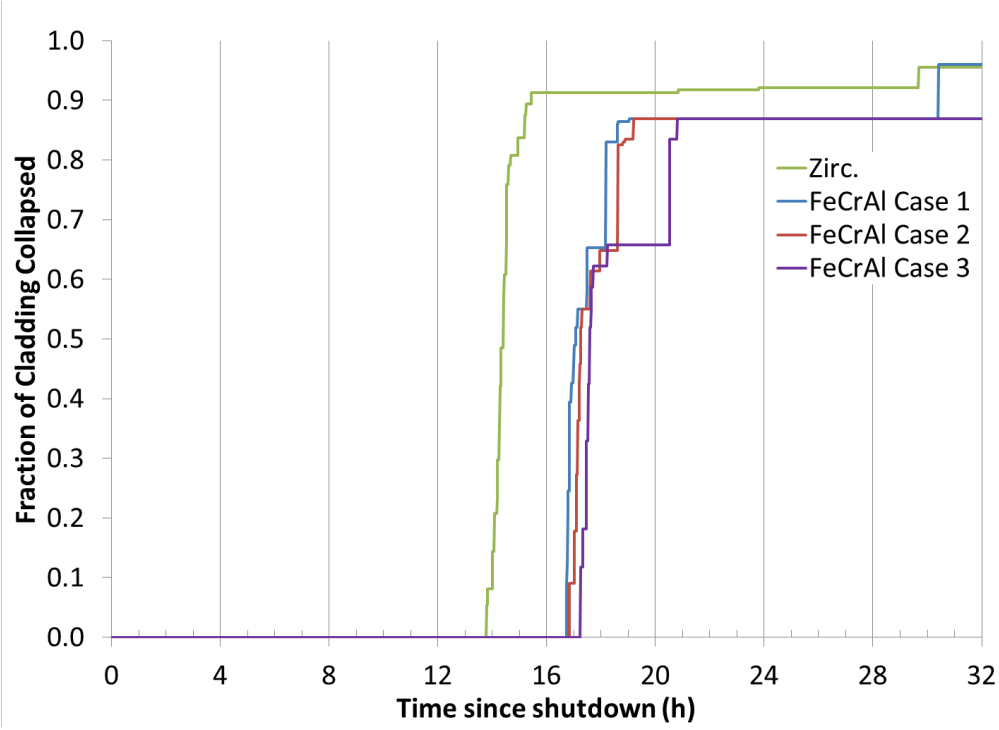

Figure 20. LTSBO 8h DC Loss - Fraction of Cladding Collapsed

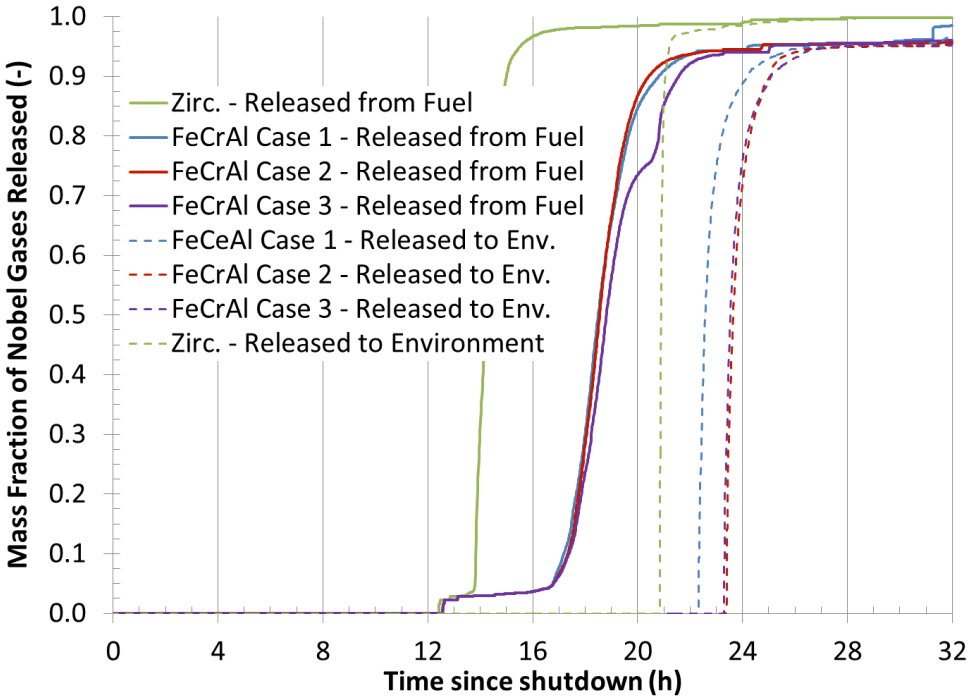

Figure 21. LTSBO 8h DC Loss - Fraction of Nobel Gases Released

4.3 UNMITIGATED LTSBO WITH DC LOSS AT 16H

The figures of merit results for the cases are summarized in Table 12. Figure 22 through Figure 27 depict the reactor and containment pressure, RPV water level, peak intact cladding temperature, total and in-vessel hydrogen generation, fraction of cladding collapsed, and the fraction of noble gas released.

During this unmitigated LTSBO, the operators have DC power for 16 hours. As modeled, the operators depressurize the RPV at 2.9 hours by manually actuating a SRV due to high temperatures in the suppression chamber. The RCIC or HPCI operate until 4.4 hours when they are isolated due to low steam pressure. After cessation of water injection, the RPV water level continuously drops while the water boils away. With 16 hours of DC power, the SRV stays open during this time, limiting the pressure of the RPV, and closes after lower head failure. Compared to the accident scenario in Section 4.2, the RPV remains at low pressure and the water level doesn't temporarily swell during boil down. This contributes to faster boil down of the RPV water level in this scenario. As the water boils away, the fuel becomes uncovered and begins to heat up. The Zircaloy cladding heats up faster than the FeCrAl cladding due to the oxidation kinetics. Despite its higher failure temperature, the Zircaloy cladding begins to relocate sooner than the FeCrAl cladding. The core debris relocates downward, eventually into the RPV lower head. The lower head dries out faster in the Zircaloy case than in the FeCrAl case. However, the lower head is predicted to fail slightly later in the Zircaloy case than in the FeCrAl case. The melt relocates to the drywell where core debris-concrete interaction is predicted to occur. The containment is predicted to fail slightly later in the Zircaloy case than in the FeCrAl case. Soon after containment failure, deflagrations are predicted to occur in containment and noble gases (and other radioactive fission products) are released to the environment.

When comparing the figures of merit, Table 12, of FeCrAl Case 2 to the base case Zircaloy system, the onset of hydrogen generation is delayed 31 minutes. The timing to first release of the radionuclides in the gap is delayed only 7 minutes. The generation of substantial quantities of hydrogen (taken as 100 kg) is delayed by 50 minutes. The timing to initial melting of the metallic cladding is delayed 43 minutes and the initial collapse of a cladding segment is delayed 42 minutes.

After the onset of fuel damage the lower head is predicted to fail 73 minutes sooner. The failure of containment, deflagrations in the reactor building, and the onset of radionuclide release into the environment are predicted to occur 14, 7, and 15 minutes sooner, respectively. FeCrAl Case 2 produces less hydrogen (i.e. 32% less) and carbon monoxide (i.e. 21% less) by 32 hours.

Table 12. Figure of Merit Results for Unmitigated Long Term Station Blackout – 16h

Figure of merit	Zirc.	FeCrAl Case 2
0.5 kg of H_2 is generated[a]	611	642
First fuel failure (gap release)[a]	613	620
100 kg of H_2 is generated[a]	639	689
First cladding metal melting[a]	644	687
First cladding collapse[a]	659	701
Lower head failure[a]	1,088	1,015
Containment failure[a]	1,217	1,203
First deflagration in building[a]	1,217	1,210
0.5 kg noble gas release to environment[a]	1,219	1,204
H_2 gas generated at 32 h[b]	1,764	1,195
CO gas generated at 32 h[b]	20,290	16,000

[a] = *minute* [b] = *kg*

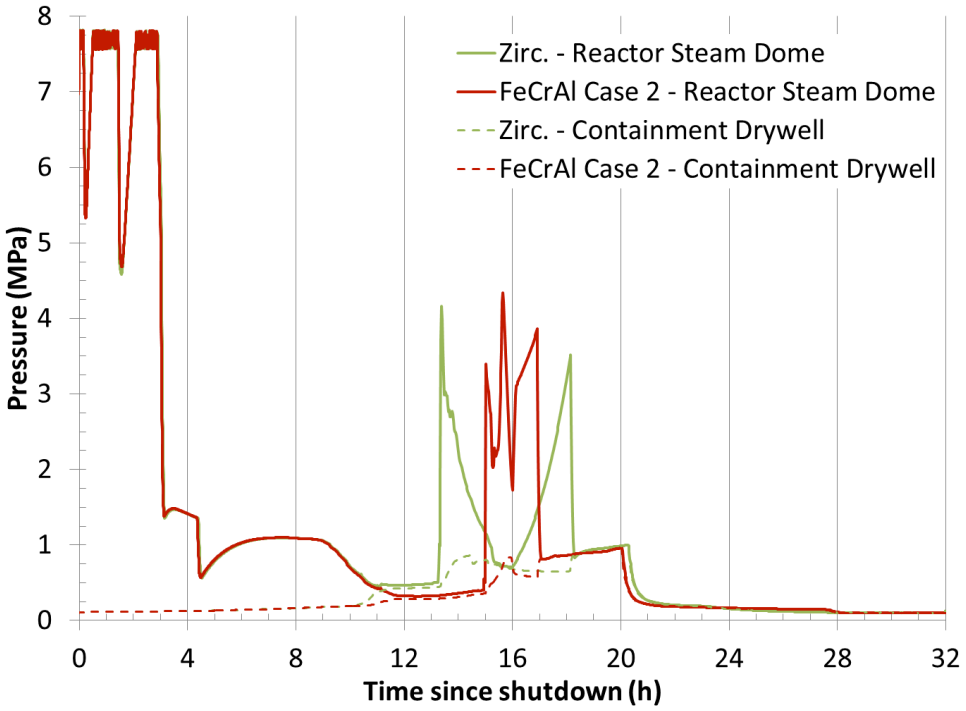

Figure 22. LTSBO 16h DC Loss - Reactor and Drywell Pressure

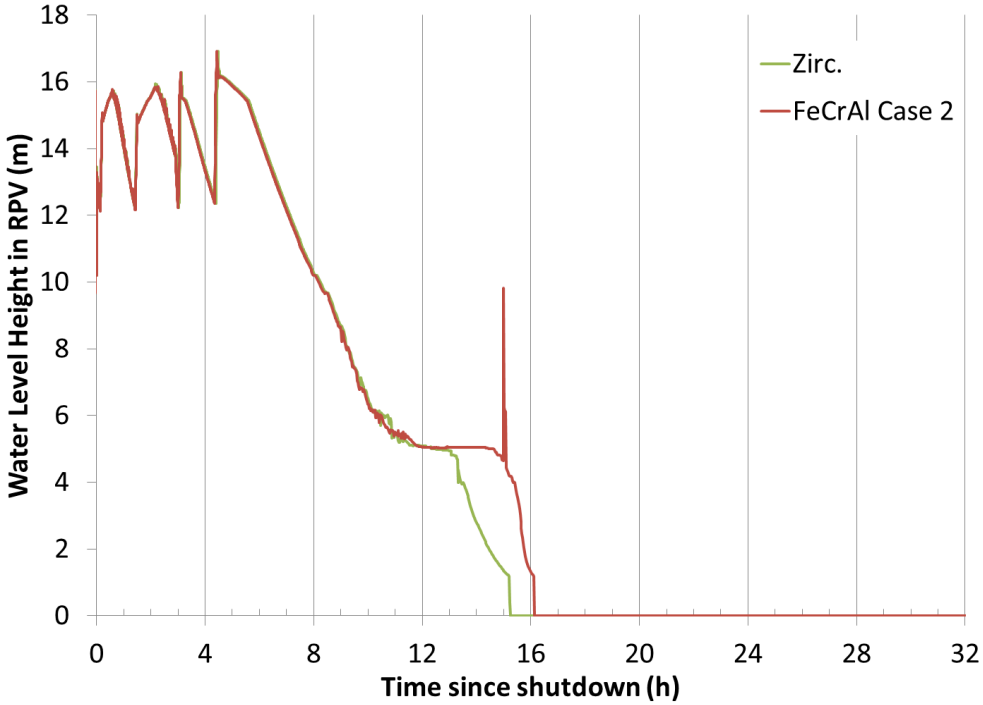

Figure 23. LTSBO 16h DC Loss - RPV Water Level

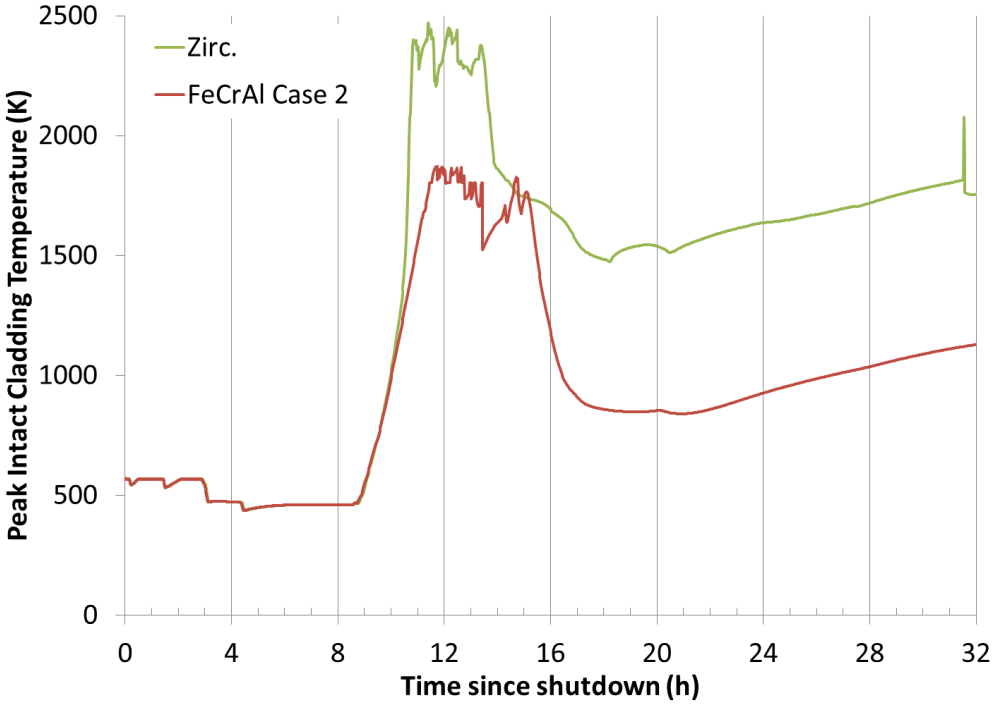

Figure 24. LTSBO 16h DC Loss - Peak Intact Cladding Temperature

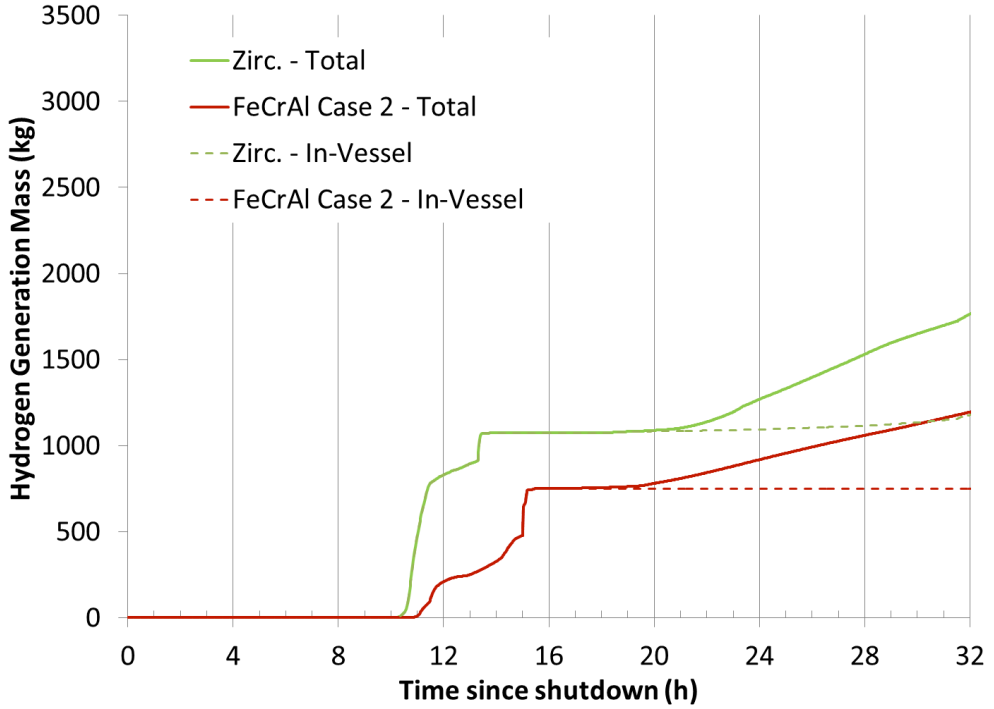

Figure 25. LTSBO 16h DC Loss - Total and In-Vessel Hydrogen Generation

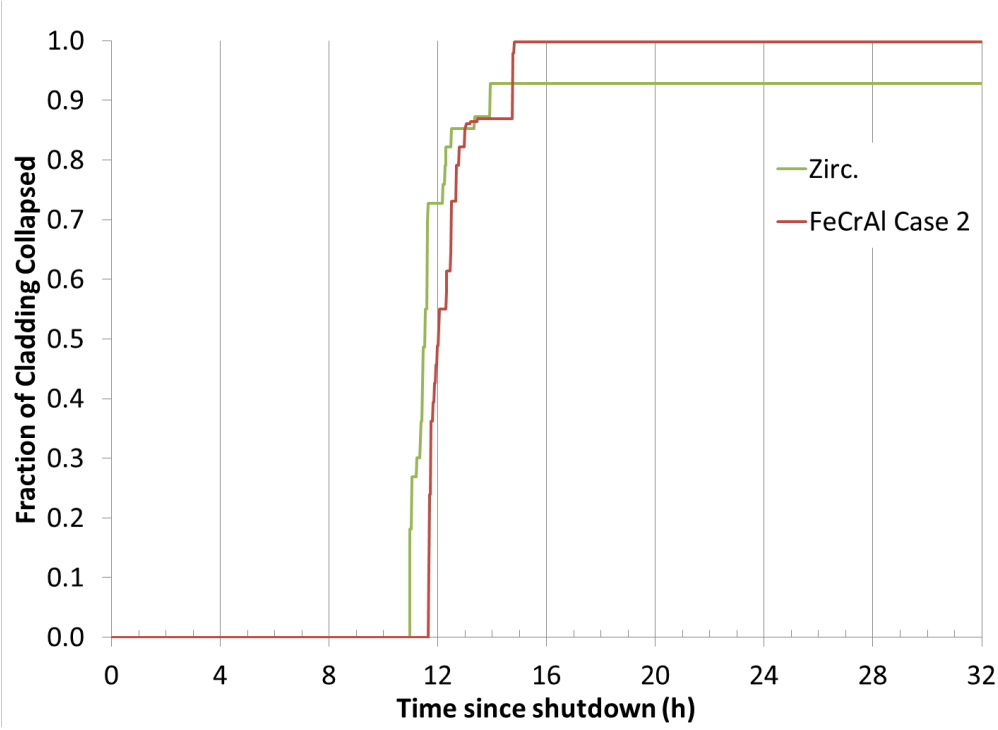

Figure 26. LTSBO 16h DC Loss - Fraction of Cladding Collapsed

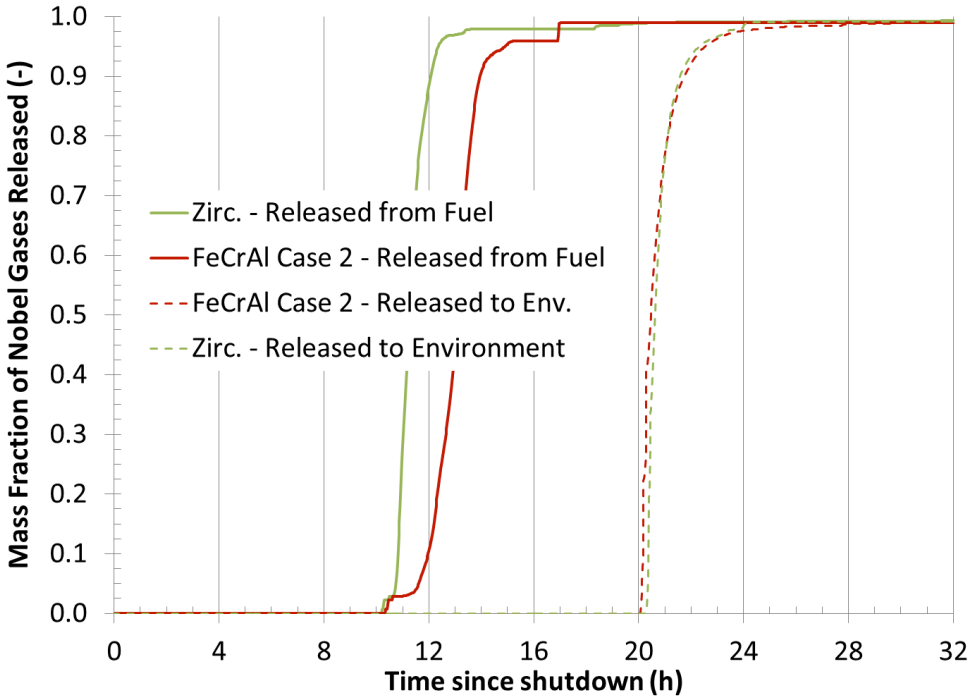

Figure 27. LTSBO 16h DC Loss - Fraction of Nobel Gases Released

4.4 SBO WITH MITIGATION LOSS AT 16H

The figures of merit results for the cases are summarized in Table 13. Figure 28 through Figure 33 depict the reactor and containment pressure, RPV water level, peak intact cladding temperature, total and in-vessel hydrogen generation, fraction of cladding collapsed, and the fraction of noble gas released.

During this SBO, the operators have DC power for 16 hours. As modeled, the operators depressurize the RPV at 2.9 hours by manually actuating a SRV due to high temperatures in the suppression chamber. The RCIC or HPCI operate until 4.4 hours when they are isolated due to low steam pressure. At 5 hours, water injection starts by an external source through the feedwater line at 454 liters per minute (120 GPM). This water injection is maintained until the 16-hour point.

At 16 hours, DC power and external water injection are lost, the manually controlled SRV closes, and the RPV repressurizes up to the lowest automatic set point of the SRVs. As the RPV repressurizes, the water level briefly swells and then resumes boiling away. Eventually, the fuel become uncovered and begins to heat up. The Zircaloy cladding heats up faster than the FeCrAl cladding due to the oxidation kinetics. Despite its higher failure temperature, the Zircaloy cladding begins to relocate much sooner than the FeCrAl cladding. The containment is predicted to fail earlier in the Zircaloy case than in the FeCrAl cases. The earlier hydrogen generation and heat generated during oxidation of the Zircaloy contributes to the earlier pressurization and failure of containment. Soon after containment failure, deflagrations are predicted to occur in containment and noble gases (and other radioactive fission products) are released to the environment. The core debris relocates downward, eventually into the RPV lower head. The lower head dries out and fails faster in the Zircaloy case than in the FeCrAl cases. The melt relocates to the drywell where core debris-concrete interaction is predicted to occur.

When comparing the figures of merit, Table 13, of FeCrAl Case 2 to the base case Zircaloy system, the onset of hydrogen generation is delayed 89 minutes. The timing to first release of the radionuclides in the gap is delayed 12 minutes. The generation of substantial quantities of hydrogen (taken as 100 kg) is delayed by 249 minutes. The timing to initial melting of the metallic cladding is delayed 240 minutes and the initial collapse of a cladding segment is delayed 242 minutes.

After the onset of fuel damage, containment failure, the onset of deflagrations and radionuclide release to the environment are delayed 313, 318, and 315 minutes, respectively. Failure of the lower head occurs late and delayed 24 minutes. FeCrAl Case 2 produces less hydrogen (i.e. 20% less) by 32 hours. Negligible carbon monoxide is generated by either case by 32 hours.

Table 13. Figure of Merit Results for SBO with Mitigation Loss at 16h

Figure of merit	Zirc.	FeCrAl Case 2
0.5 kg of H_2 is generated[a]	1,412	1,501
First fuel failure (gap release)[a]	1,420	1,432
100 kg of H_2 is generated[a]	1,475	1,724
First cladding metal melting[a]	1,523	1,763
First cladding collapse[a]	1,527	1,769
Lower head failure[a]	2,231	2,255
Containment failure[a]	1,627	1,940
First deflagration in building[a]	1,627	1,945
0.5 kg noble gas release to environment[a]	1,627	1,942
H_2 gas generated at 32 h[b]	1,861	1,480
CO gas generated at 32 h[b]	7	5

[a] = *minute* [b] = *kg*

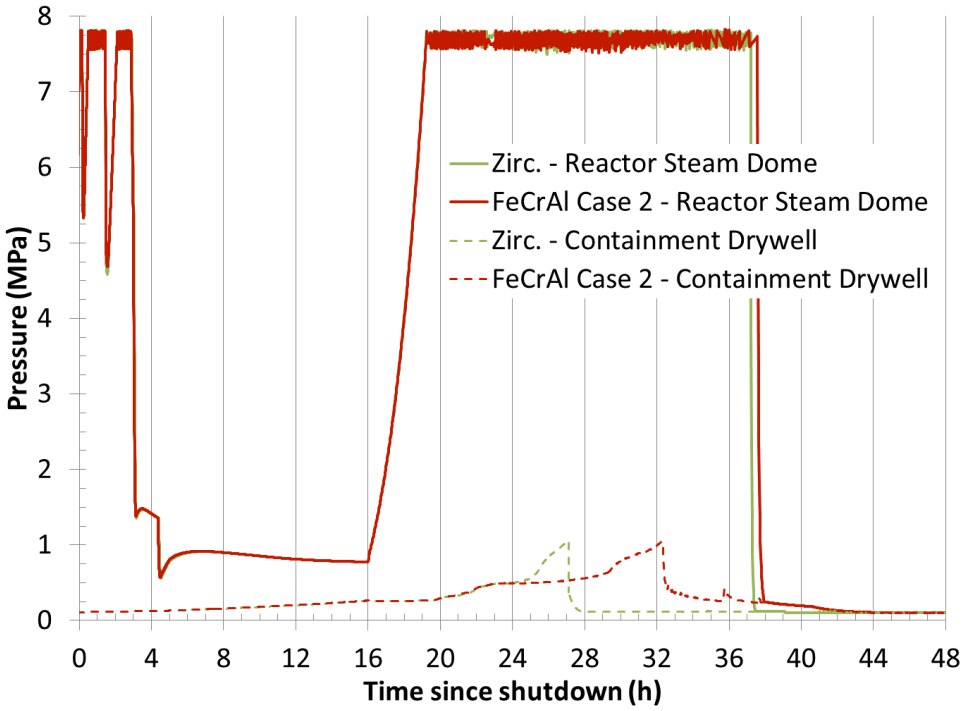

Figure 28. SBO 16h Mitigation Loss - Reactor and Drywell Pressure

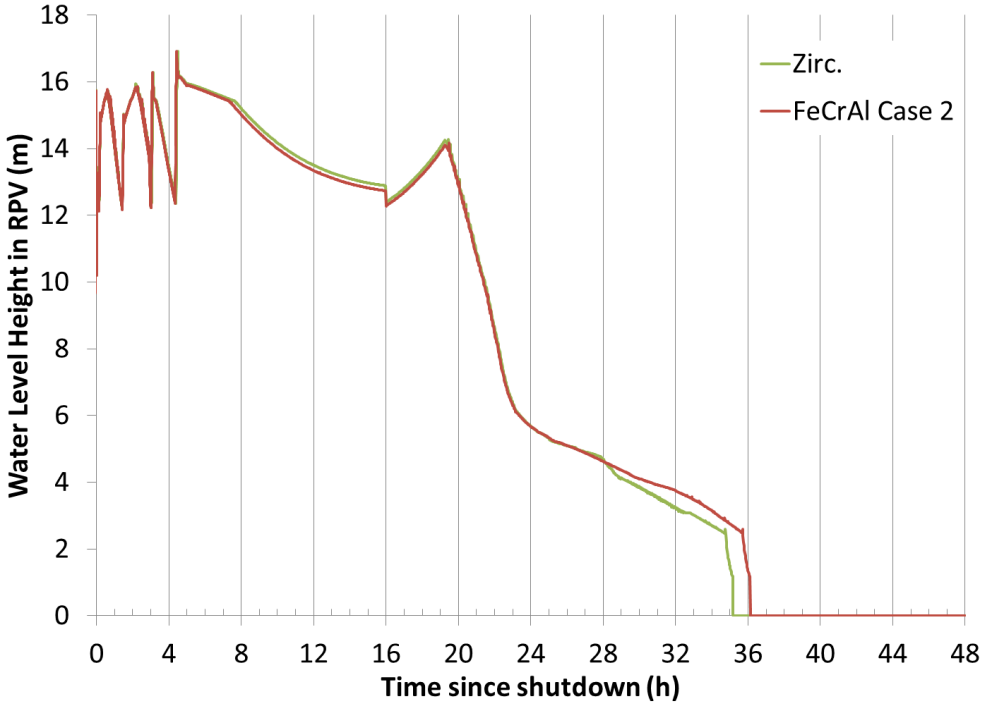

Figure 29. SBO 16h Mitigation Loss - RPV Water Level

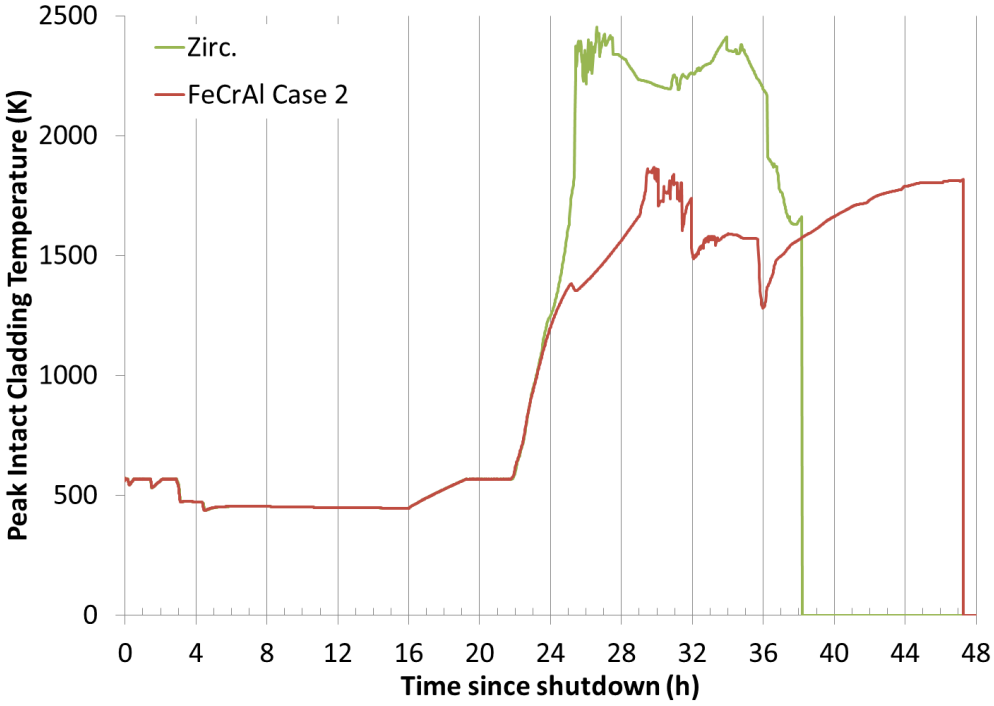

Figure 30. SBO 16h Mitigation Loss - Peak Intact Cladding Temperature

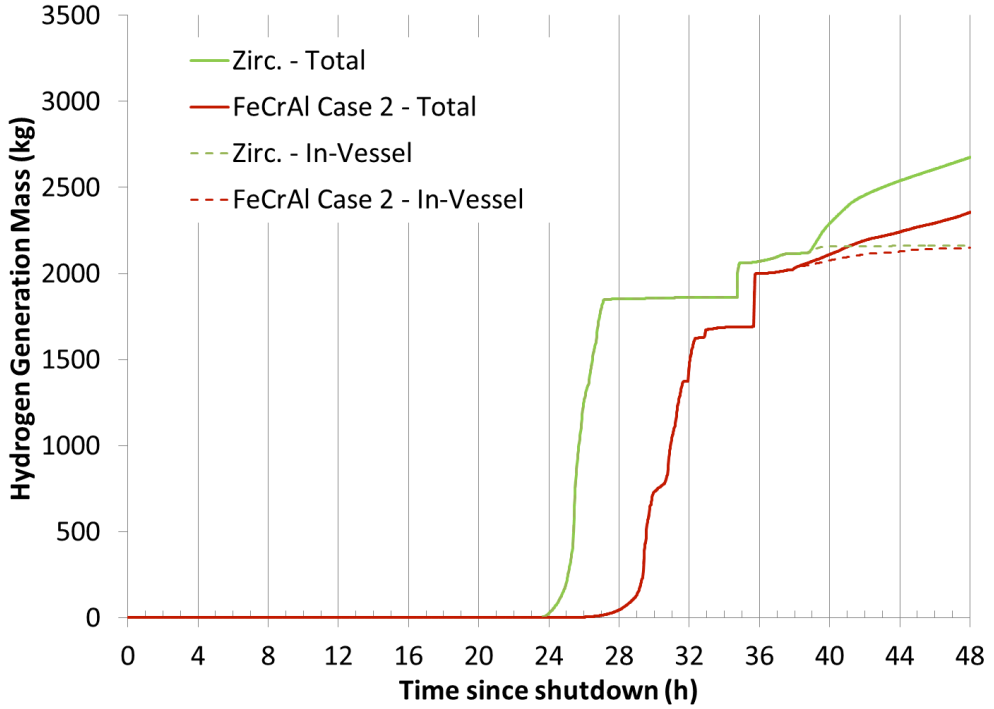

Figure 31. SBO 16h Mitigation Loss - Total and In-Vessel Hydrogen Generation

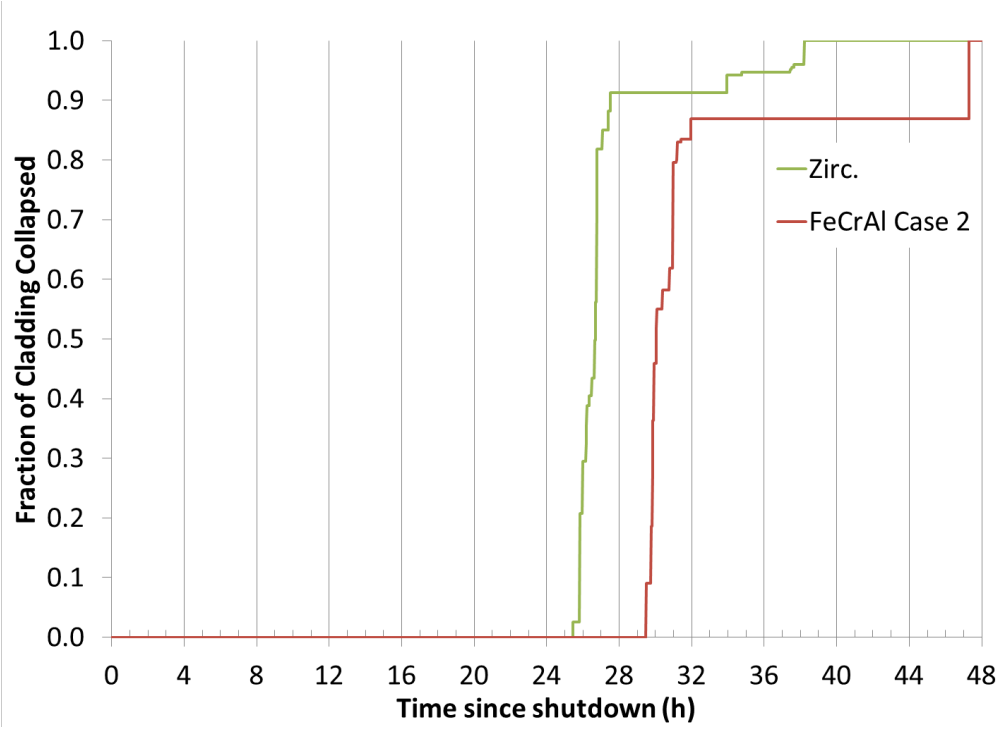

Figure 32. SBO 16h Mitigation Loss - Fraction of Cladding Collapsed

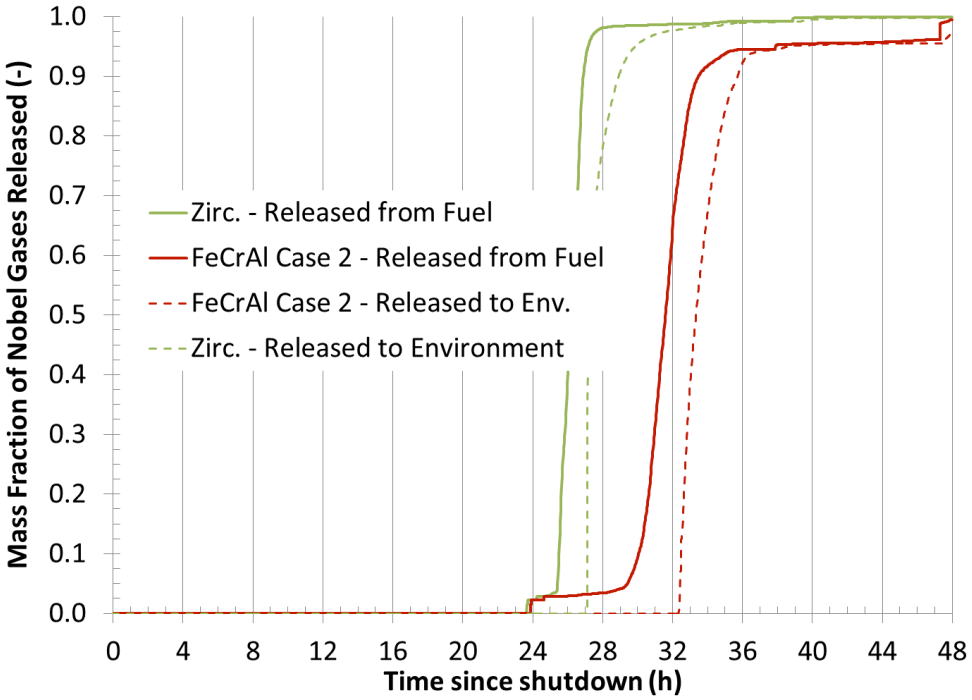

Figure 33. SBO 16h Mitigation Loss - Fraction of Nobel Gases Released

4.5 SBO WITH MITIGATION LOSS AT 24H

The figures of merit results for the cases are summarized in Table 14. Figure 34 through Figure 39 depict the reactor and containment pressure, RPV water level, peak intact cladding temperature, total and in-vessel hydrogen generation, fraction of cladding collapsed, and the fraction of noble gas released.

During this SBO, the operators have DC power for 24 hours. As modeled, the operators depressurize the RPV at 2.9 hours by manually actuating a SRV due to high temperatures in the suppression chamber. The RCIC or HPCI operate until 4.4 hours when they are isolated due to low steam pressure. At 5 hours, water injection starts by an external source through the feedwater line at 454 liters per minute (120 GPM). This water injection is maintained until the 24-hour point.

At 24 hours, DC power and external water injection are lost, the manually controlled SRV closes, and the RPV repressurizes up to the lowest automatic set point of the SRVs. As the RPV repressurizes, the water level briefly swells and then resumes boiling away. Eventually, the fuel become uncovered and begins to heat up. The Zircaloy cladding heats up faster than the FeCrAl cladding due to the oxidation kinetics. Despite its higher failure temperature, the Zircaloy cladding begins to relocate much sooner than the FeCrAl cladding. The containment is predicted to fail earlier in the Zircaloy case than in the FeCrAl cases. The earlier hydrogen generation and heat generated during oxidation of the Zircaloy contributes to the earlier pressurization and failure of containment. Soon after containment failure, deflagrations are predicted to occur in containment for the Zircaloy case. Interestingly, deflagrations are not predicted to occur in the FeCrAl case. Soon after containment failure, noble gases (and other radioactive fission products) are released to the environment for both cases. The simulation ended before lower head failure for both cases. Thus, no core debris-concrete interaction is predicted to occur and all hydrogen is generated in-vessel.

When comparing the figures of merit, Table 14, of FeCrAl Case 2 to the base case Zircaloy system, the onset of hydrogen generation is delayed 101 minutes. The timing to first release of the radionuclides in the gap is delayed 15 minutes. The generation of substantial quantities of hydrogen (taken as 100 kg) is delayed by 290 minutes. The timing to initial melting of the metallic cladding is delayed 254 minutes and the initial collapse of a cladding segment is delayed 282 minutes.

After the onset of fuel damage, containment failure and radionuclide release to the environment are delayed 282, and 277 minutes, respectively. Failure of the lower head is not predicted to occur within 42 hours for both simulations. No hydrogen or carbon monoxide is generated by either case by 32 hours. By the end of the simulation, 42 hours, the FeCrAl case had generated 44% less hydrogen compared to the Zircaloy case.

Table 14. Figure of Merit Results for SBO with Mitigation Loss at 24h

Figure of merit	Zirc.	FeCrAl Case 2
0.5 kg of H_2 is generated[a]	1,967	2,068
First fuel failure (gap release)[a]	1,976	1,991
100 kg of H_2 is generated[a]	2,037	2,327
First cladding metal melting[a]	2,118	2,372
First cladding collapse[a]	2,120	2,402
Lower head failure[a]	NA	NA
Containment failure[a]	2,146	2,423
First deflagration in building[a]	2,146	NA
0.5 kg noble gas release to environment[a]	2,146	2,426
H_2 gas generated at 32 h[b]	0	0
CO gas generated at 32 h[b]	0	0

[a] = minute [b] = kg NA=Not Applicable (Before end of Simulation)

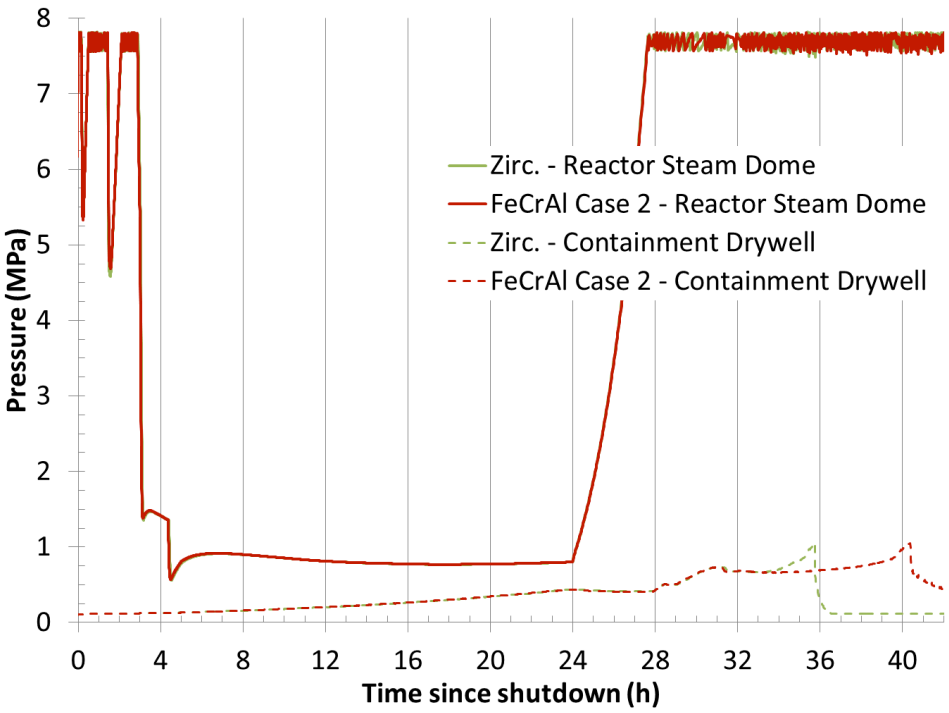

Figure 34. SBO 24h Mitigation Loss - Reactor and Drywell Pressure

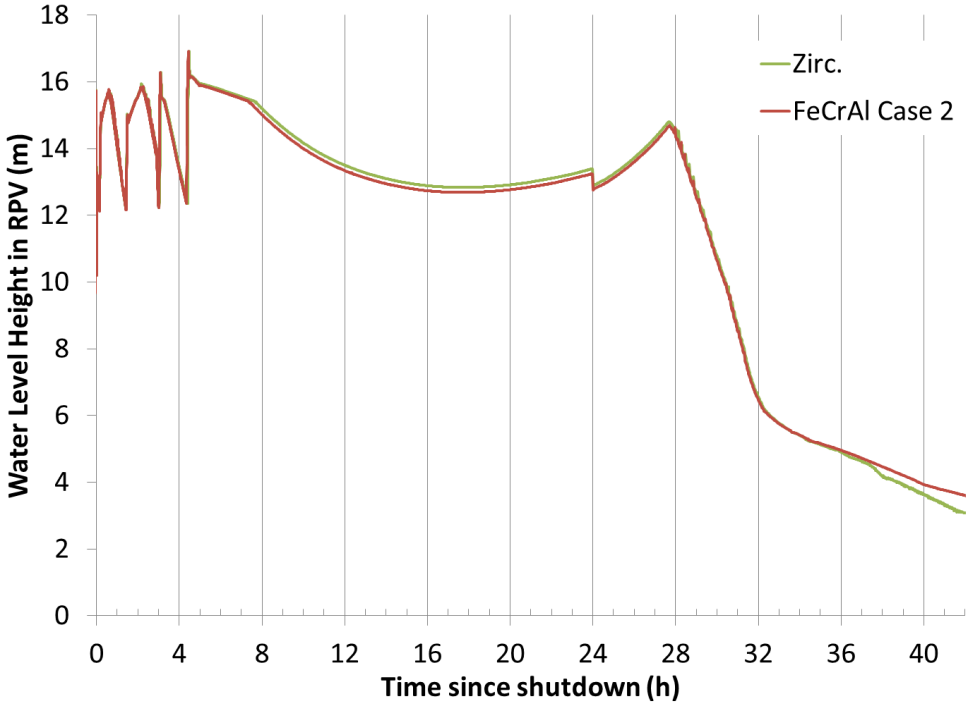

Figure 35. SBO 24h Mitigation Loss - RPV Water Level

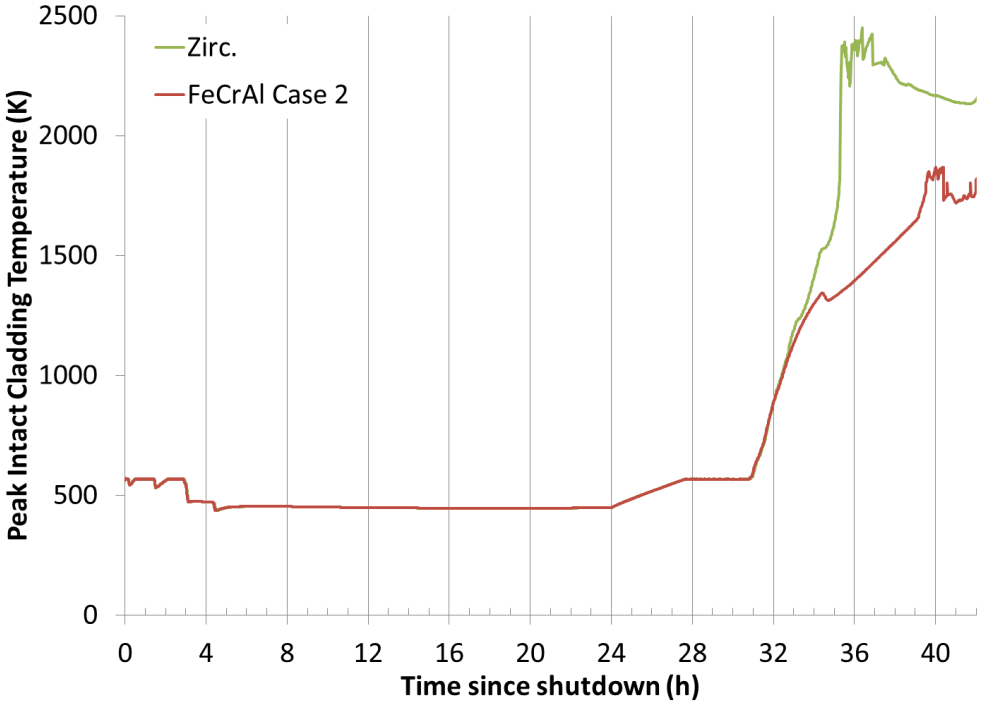

Figure 36. SBO 24h Mitigation Loss - Peak Intact Cladding Temperature

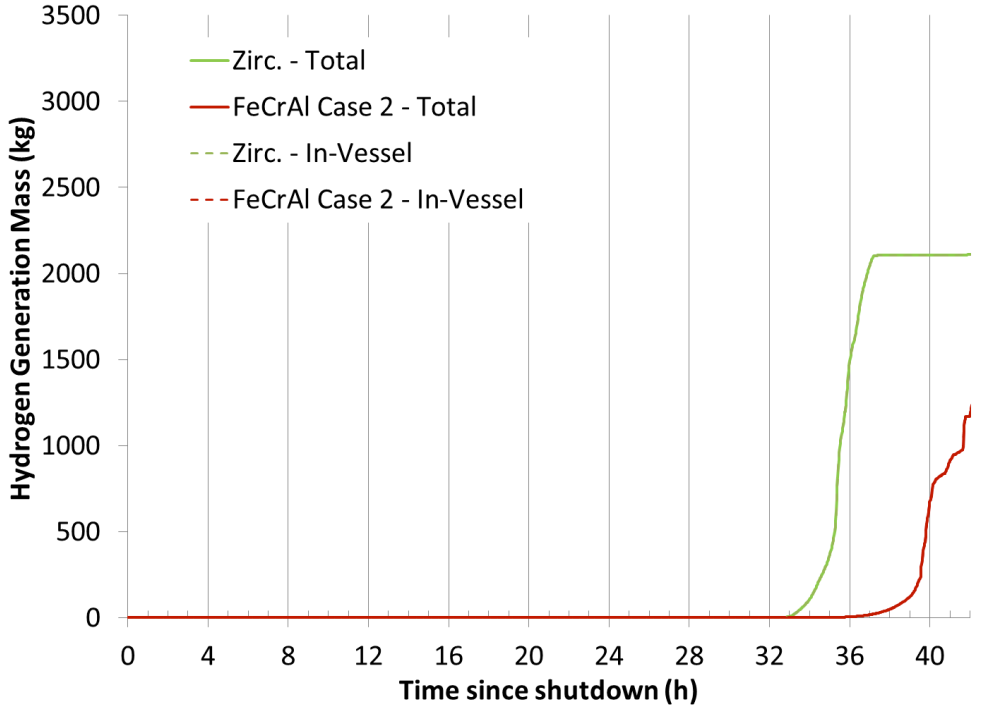

Figure 37. SBO 24h Mitigation Loss - Total and In-Vessel Hydrogen Generation

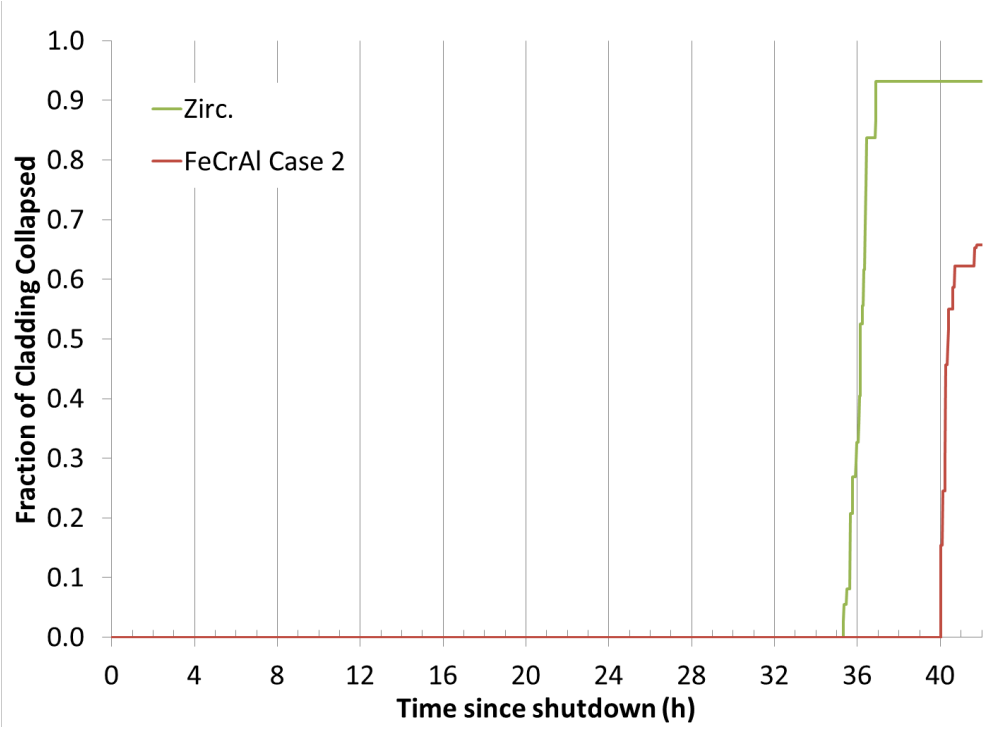

Figure 38. SBO 24h Mitigation Loss - Fraction of Cladding Collapsed

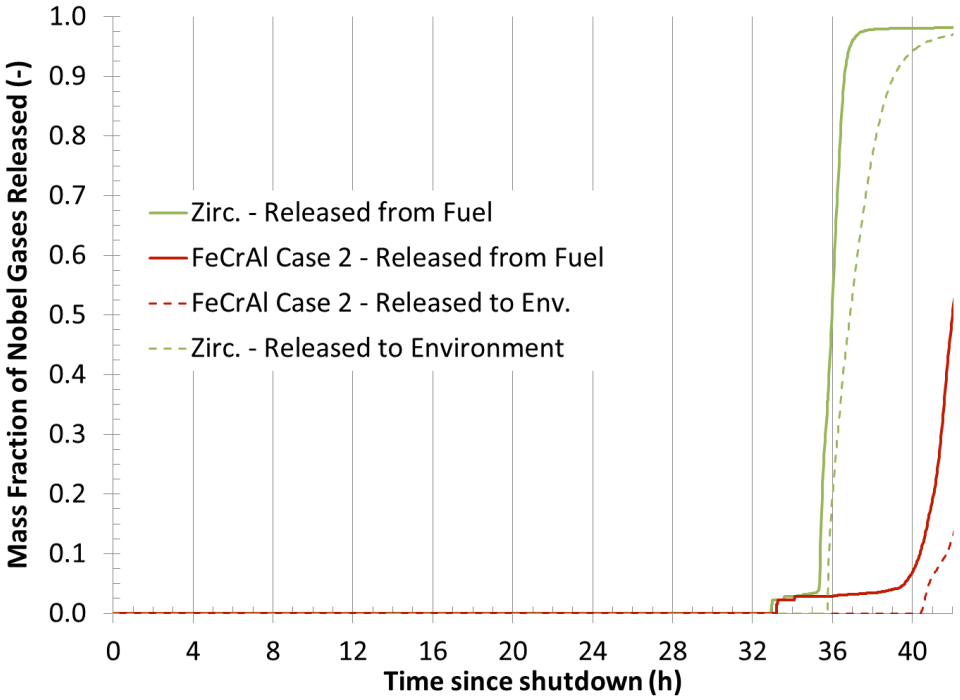

Figure 39. SBO 24h Mitigation Loss - Fraction of Nobel Gases Released

4.6 MITIGATED STSBO

The figures of merit results for the cases are summarized in Table 15. Figure 40 through Figure 45 depict the reactor and containment pressure, RPV water level, peak intact cladding temperature, total and in-vessel hydrogen generation, fraction of cladding collapsed, and the fraction of noble gas released.

During this STSBO, there are no operator actions or water injection initially by the RCIC, HPCI, or external means. Without operator actuation of the SRVs or the HPCI operating, the RPV remains pressurized. The water in the RPV boils away eventually uncovering the fuel. The fuel then begins to heat up and oxidize. At 2 hours, water injection starts by an external source through the feedwater line at 568 liters per minute (150 GPM). This water injection is maintained throughout the rest of the simulation. The water injection is sufficient to reflood the core. For the Zircaloy case, the rapid oxidation results in heatup and collapse of much of the fuel. In contrast, no FeCrAl cladding is predicted to collapse during the simulation. For both cases, the core is reflooded and the accident is stabilized before lower head or containment failure.

When comparing the figures of merit, Table 15, of FeCrAl Case 2 to the base case Zircaloy system, the onset of hydrogen generation is delayed 39 minutes. The timing to first release of the radionuclides in the gap is delayed only 4 minutes. Only 91 kg of hydrogen are generated in the FeCrAl case whereas 1445 kg are generated by the Zircaloy case. No cladding failure is predicted to occur in the FeCrAl case, in contrast to the Zircaloy case. For both simulations, negligible carbon monoxide is generated by 32 hours as core debris does not leave the vessel to interact with the containment concrete.

Table 15. Figure of Merit Results for Mitigated STSBO

Figure of merit	Zirc.	FeCrAl Case 2
0.5 kg of H_2 is generated[a]	70	109
First fuel failure (gap release)[a]	72	76
100 kg of H_2 is generated[a]	97	NA
First cladding metal melting[a]	112	NA
First cladding collapse[a]	112	NA
Lower head failure[a]	NA	NA
Containment failure[a]	NA	NA
First deflagration in building[a]	NA	NA
0.5 kg noble gas release to environment[a]	NA	NA
H_2 gas generated at 32 h[b]	1445	91
CO gas generated at 32 h[b]	6	0

[a] = minute [b] = kg NA=Not Applicable

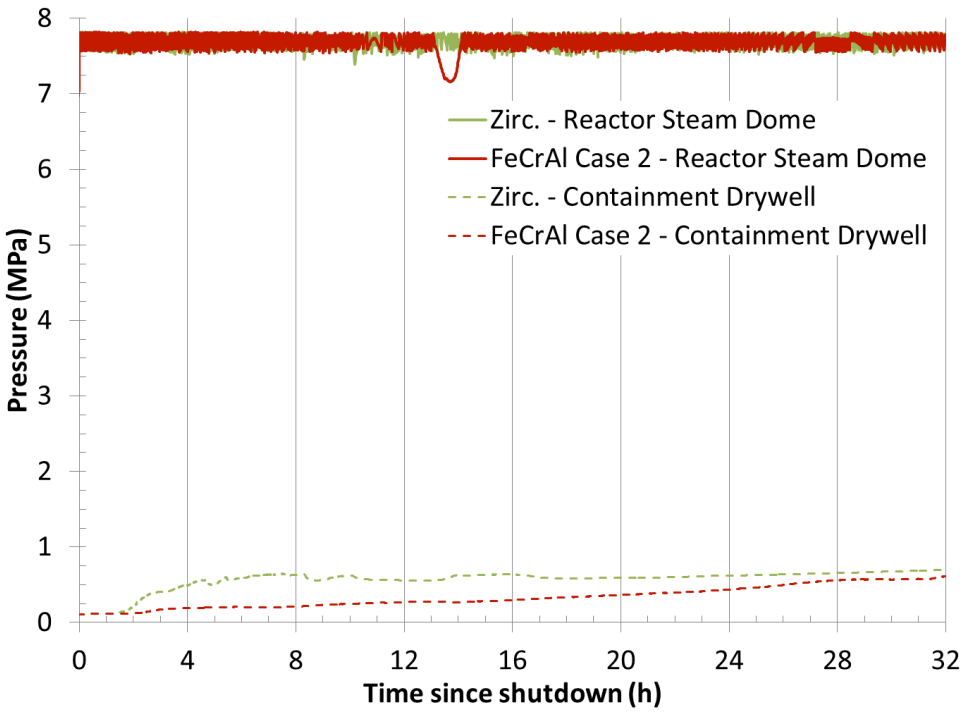

Figure 40. MSTSBO - Reactor and Drywell Pressure

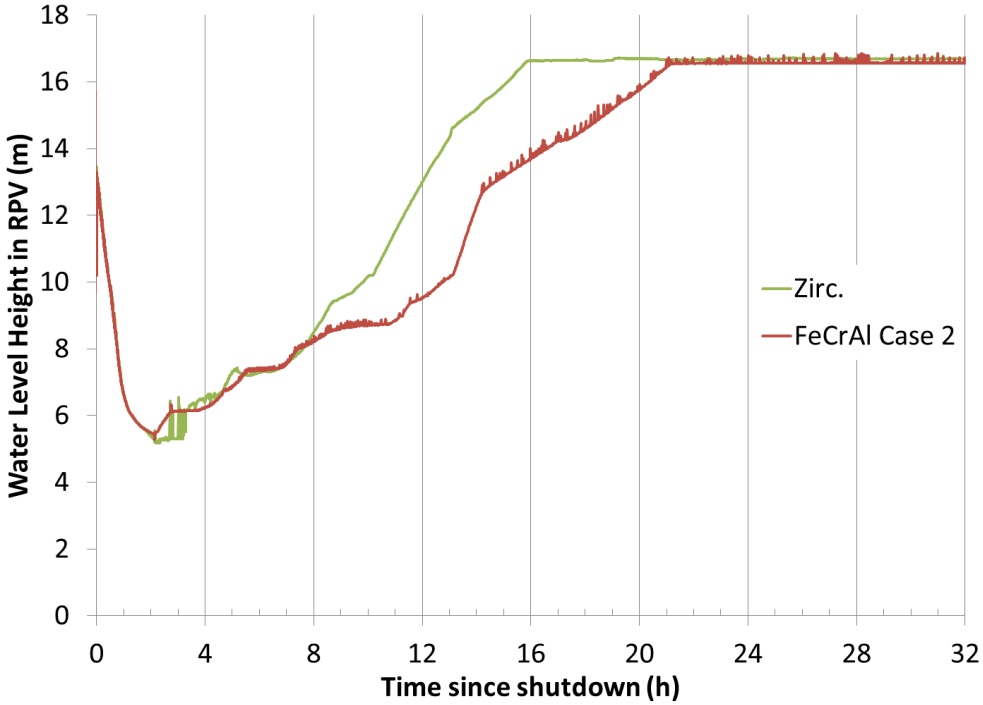

Figure 41. MSTSBO - RPV Water Level

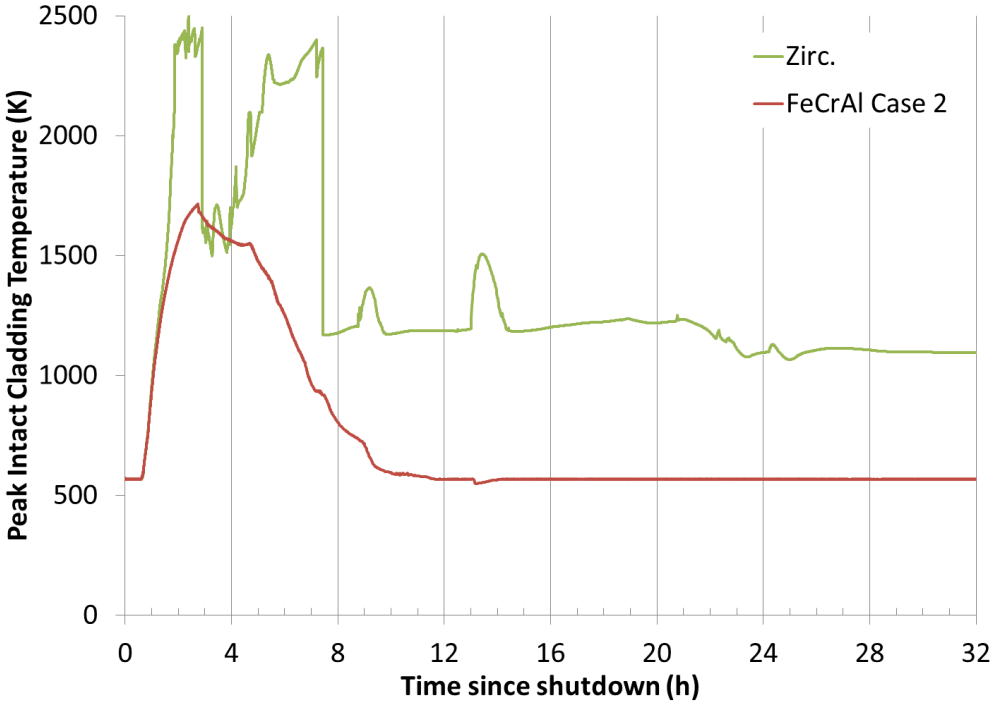

Figure 42. MSTSBO - Peak Intact Cladding Temperature

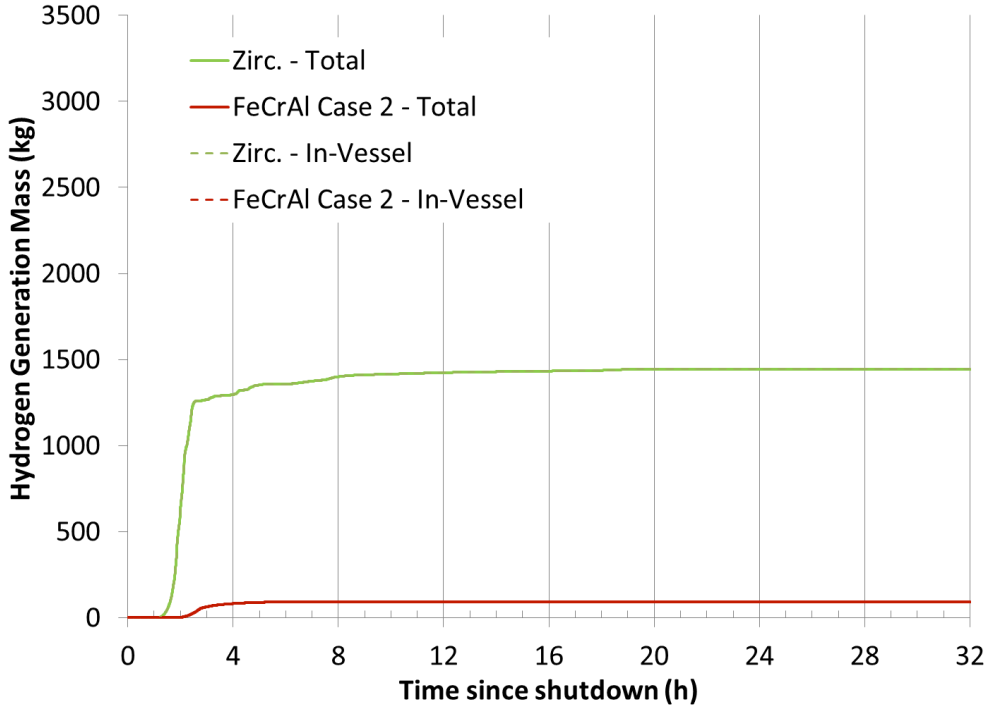

Figure 43. MSTSBO - Total and In-Vessel Hydrogen Generation

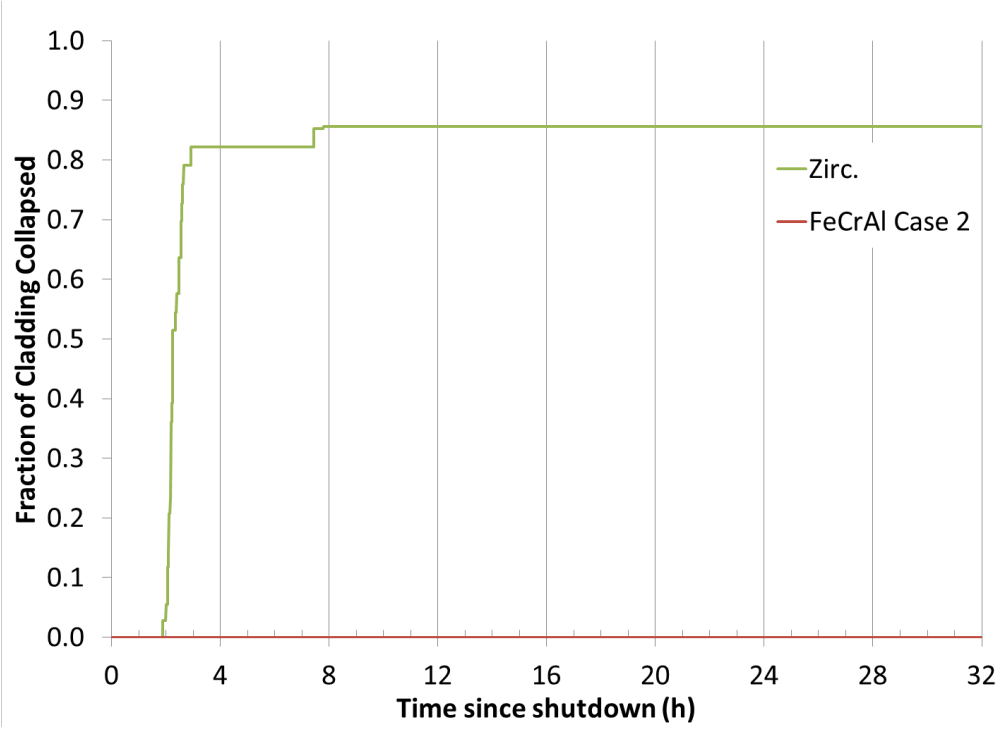

Figure 44. MSTSBO - Fraction of Cladding Collapsed

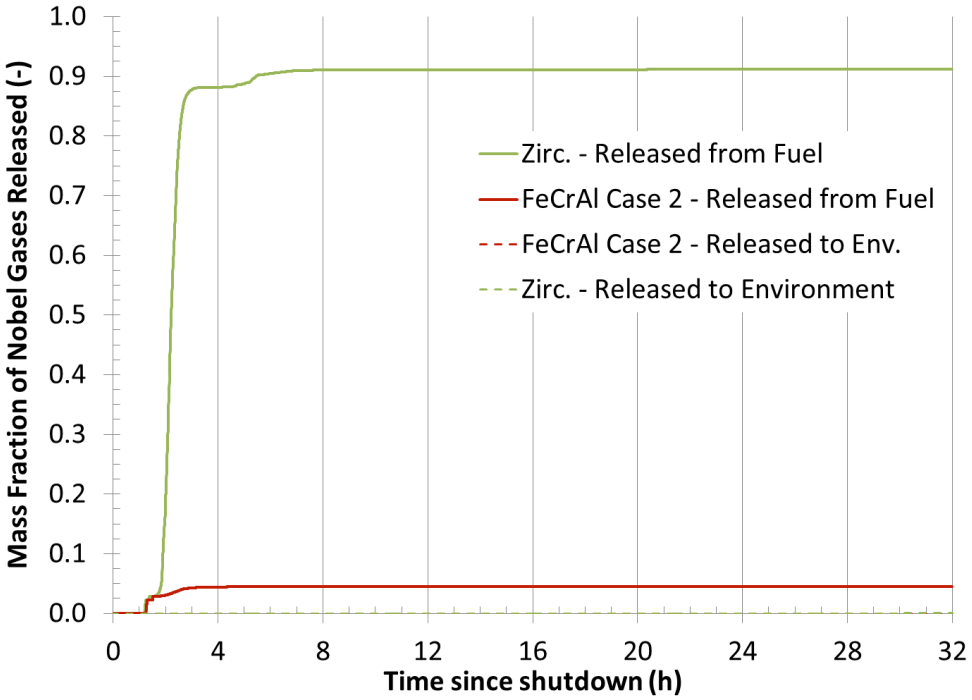

Figure 45. MSTSBO - Fraction of Nobel Gases Released

4.7 MITIGATED LTSBO

The figures of merit results for the cases are summarized in Table 16. Figure 46 through Figure 51 depict the reactor and containment pressure, RPV water level, peak intact cladding temperature, total and in-vessel hydrogen generation, fraction of cladding collapsed, and the fraction of noble gas released.

During this LTSBO, the operators have DC power for 8 hours. As modeled, the operators depressurize the RPV at 2.9 hours by manually actuating a SRV due to high temperatures in the suppression chamber. The RCIC or HPCI operate until 4.4 hours when they are isolated due to low steam pressure. After cessation of water injection, the RPV water level continuously drops while the water boils away. At 8 hours, DC power is lost, the manually controlled SRV closes, and the RPV repressurizes up to the lowest automatic set point of the SRVs. As the RPV repressurizes, the water level briefly swells and then resumes boiling away. Eventually, the fuel become uncovered and begins to heat up. The Zircaloy cladding heats up faster than the FeCrAl cladding due to the oxidation kinetics. Despite its higher failure temperature, the Zircaloy cladding begins to relocate much sooner than the FeCrAl cladding. At 16 hours, water injection starts by an external source through the feedwater line at 568 liters per minute (150 GPM). This water injection is maintained throughout the rest of the simulation. The water injection is sufficient to reflood the core. For both cases, the core is reflooded and the accident is stabilized before lower head failure. The hydrogen heat generated during oxidation of the Zircaloy contributes to the pressurization and failure of containment. Soon after containment failure, deflagrations and the onset of radionuclide releases are predicted to occur for the Zircaloy case. In contrast, containment failure is not predicted to occur before the end of the FeCrAl case simulation.

When comparing the figures of merit, Table 15, of FeCrAl Case 2 to the base case Zircaloy system, the onset of hydrogen generation is delayed 69 minutes. The timing to first release of the radionuclides in the gap is delayed only 8 minutes. The generation of substantial quantities of hydrogen (taken as 100 kg) is delayed by 188 minutes. The timing to initial melting of the metallic cladding is delayed 177 minutes and the initial collapse of a cladding segment is delayed 185 minutes.

For the Zircaloy case, containment failure, building deflagrations and the onset of radionuclide releases to the environment are predicted to occur after 19.4 hours. In contrast, containment is not predicted to fail in the FeCrAl case. FeCrAl Case 2 produces less hydrogen (i.e. 55% less) by 32 hours. For both simulations, negligible carbon monoxide is generated by 32 hours.

Table 16. Figure of Merit Results for Mitigated LTSBO

Figure of merit	Zirc.	FeCrAl Case 2
0.5 kg of H_2 is generated[a]	740	809
First fuel failure (gap release)[a]	746	754
100 kg of H_2 is generated[a]	791	979
First cladding metal melting[a]	827	1,004
First cladding collapse[a]	827	1,012
Lower head failure[a]	NA	NA
Containment failure[a]	1,162	NA
First deflagration in building[a]	1,162	NA
0.5 kg noble gas release to environment[a]	1,162	NA
H_2 gas generated at 32 h[b]	1,919	863
CO gas generated at 32 h[b]	6	5

[a] = minute [b] = kg NA=Not Applicable

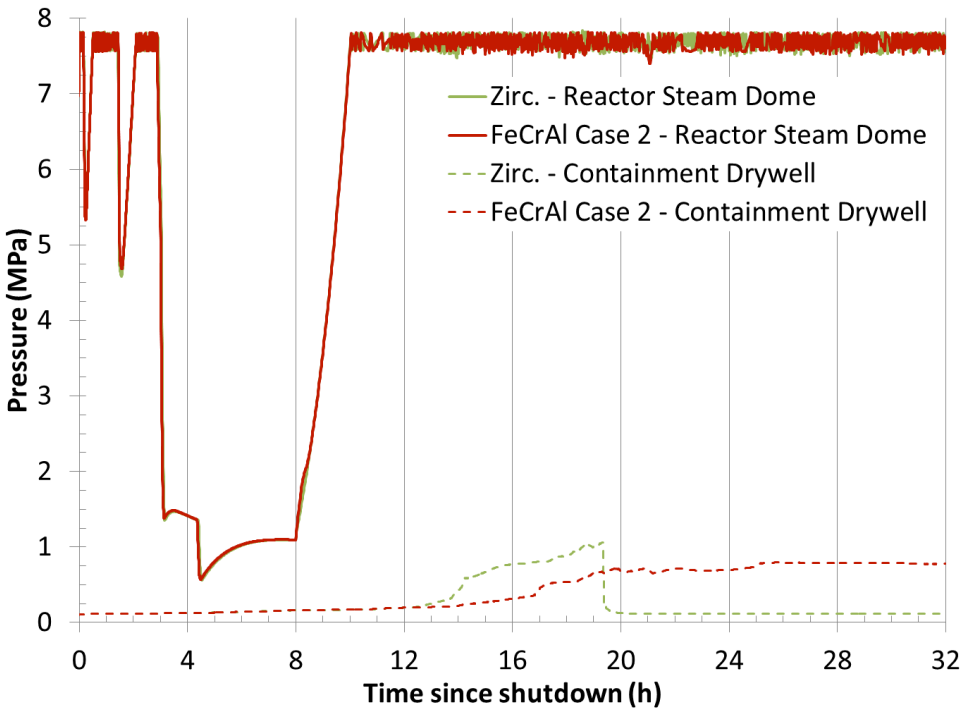

Figure 46. MLTSBO - Reactor and Drywell Pressure

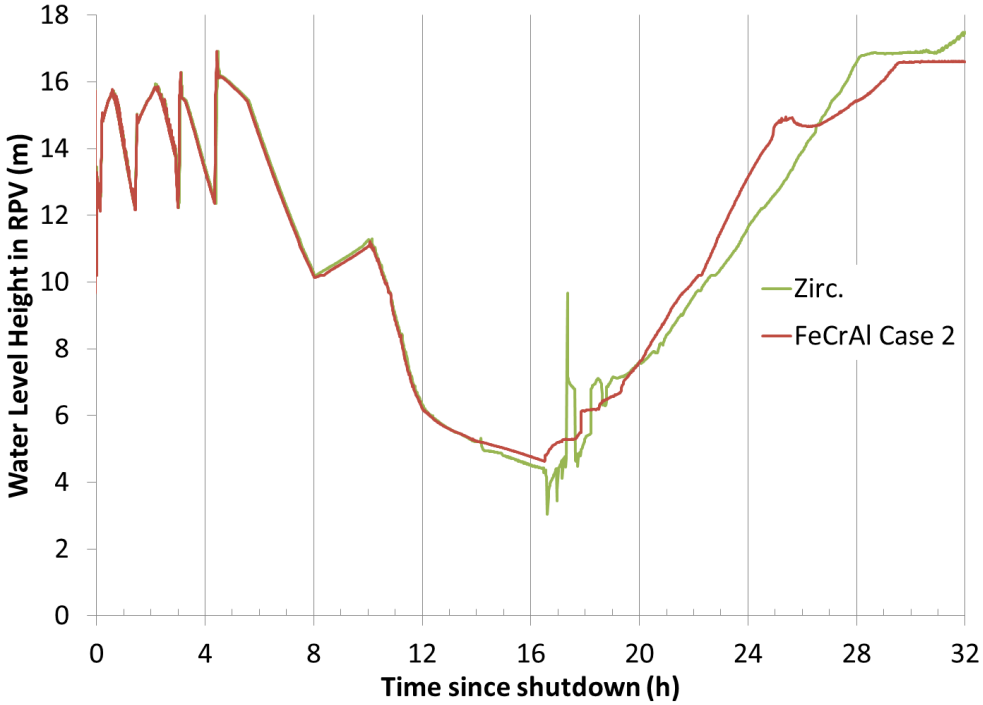

Figure 47. MLTSBO - RPV Water Level

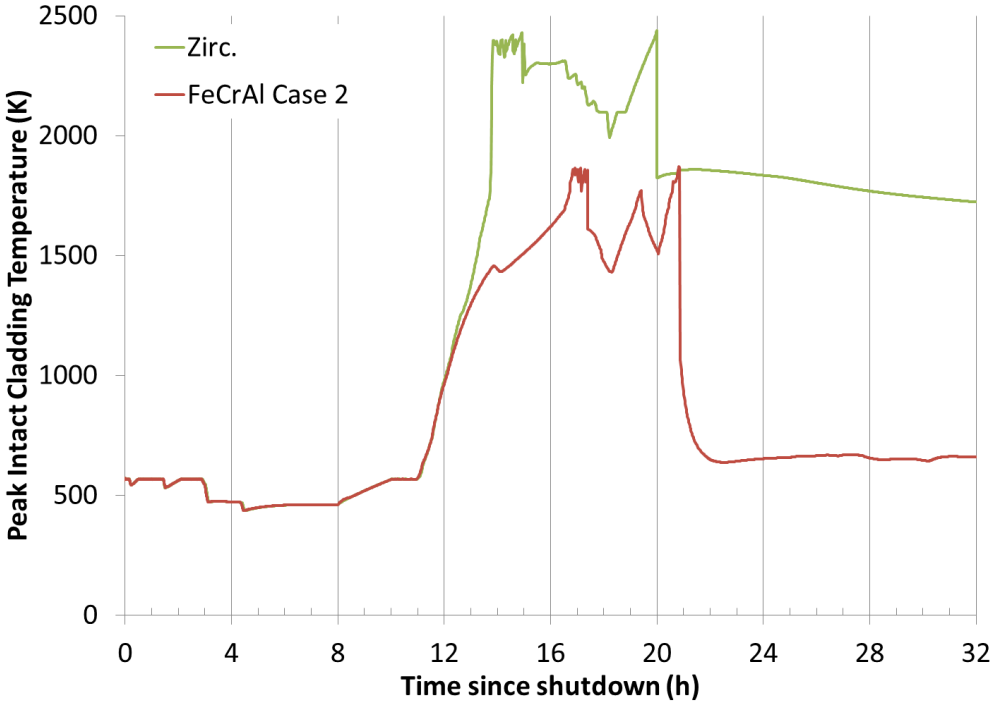

Figure 48. MLTSBO - Peak Intact Cladding Temperature

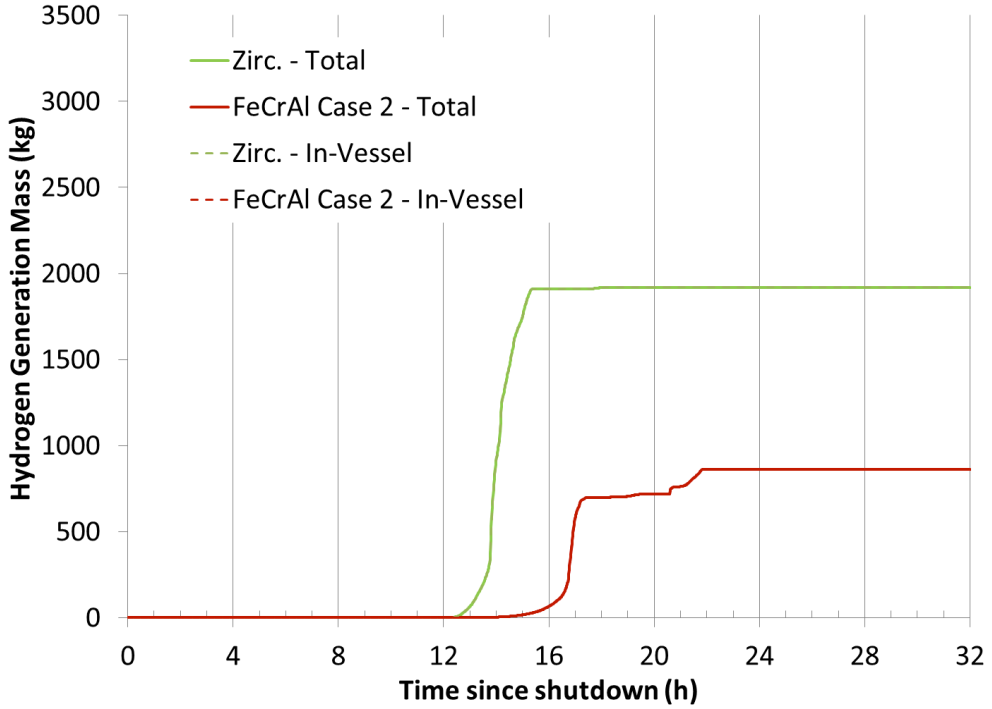

Figure 49. MLTSBO - Total and In-Vessel Hydrogen Generation

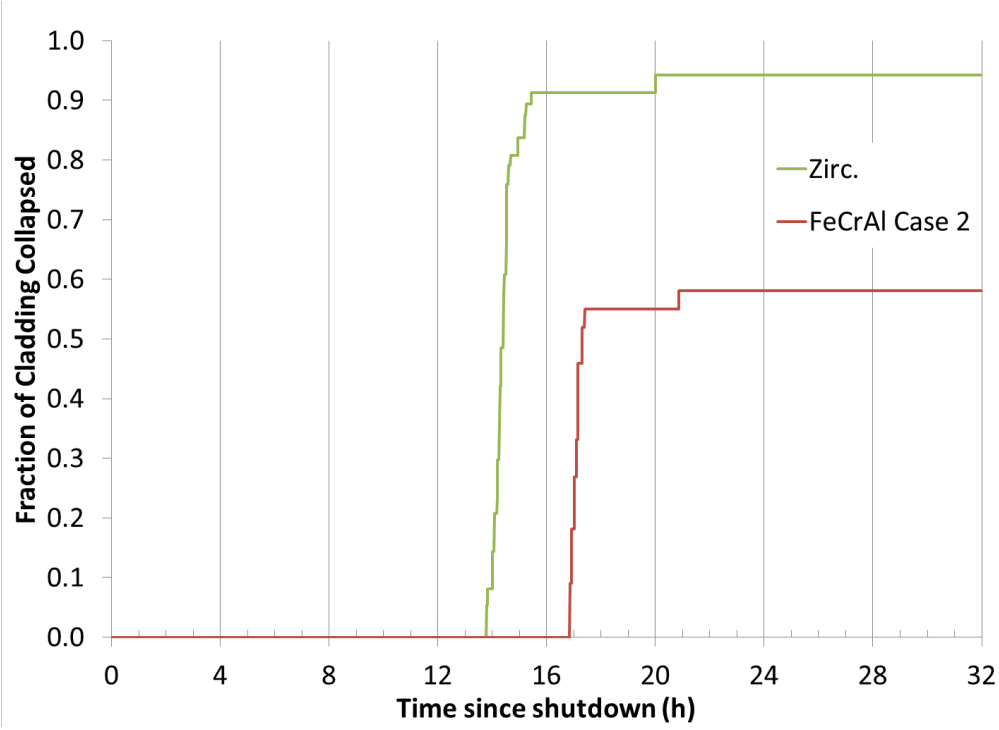

Figure 50. MLTSBO - Fraction of Cladding Collapsed

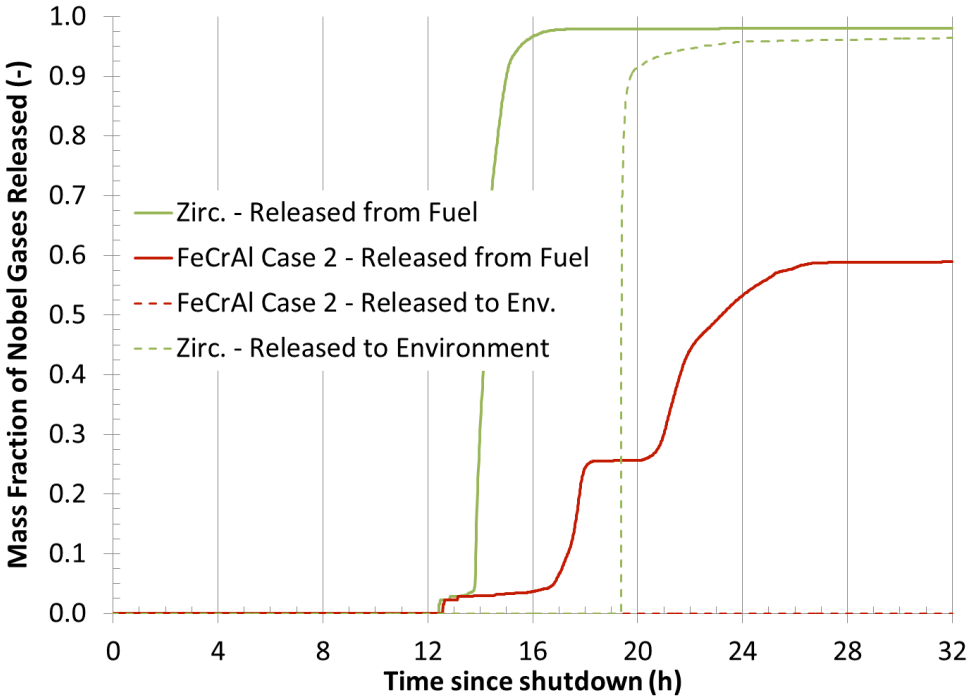

Figure 51. MLTSBO - Fraction of Nobel Gases Released

4.8 DISCUSSION OF RESULTS

Table 17 summarizes the difference in figures of merit between the FeCrAl Case 2 and Zircaloy case for the unmitigated SBO scenarios. During a station blackout with no or limited time for operator actions or restoration of long term cooling, the fuel will heat up, oxidize, fail, and relocate causing containment failure and release of radionuclides to the environment. The FeCrAl case provides some margin early in the accident progression. This ranges from 31-69 minutes for the onset of hydrogen generation to 42-183 minutes for first cladding collapse.

The timing of the lower head and containment failure was influenced by the timing and rate of boil down for the three scenarios. For fast boil down scenarios (Scenario 1) the timing of lower head and containment failure is slower for the Zircaloy case than the FeCrAl case. This is primarily driven by the differences in failure and relocation characteristics between the two claddings. For slower boil down scenarios (Scenario 2) the lower head, containment failure was delayed 1.5 and 2.5 hours, respectively, for the FeCrAl case compared to the Zircaloy case. With a slower boil down, the cladding is under steam conditions for a longer time. This increases the importance and influence the oxidation kinetics have on the accident progression. The timing and rate of boil down for Scenario 3 was in-between Scenarios 1 and 2. As such, the scenario shares core degradation and system characteristics seen in Scenarios 1 and 2. In all scenarios, less hydrogen and substantially less carbon monoxide are generated.

With respect to lower head failure timing, it should be noted that this is an area of continued uncertainty for both FeCrAl and Zircaloy [41]. There have been no prototypic tests for the BWR geometry [30].

The loss of ability to inject water is a key event during severe accidents. Table 18 is the percentage difference in timing of the events, of FeCrAl compared to the Zircaloy case, with respect to the timing of loss of water injection. For example, in Scenario 2, the loss of water injection occurs at 4.4 hours. From this point, the timing of the onset of hydrogen generation occurs 14% later in time for the FeCrAl case compared to the Zircaloy case. This provides another measure as to the additional time operators have to restore water injection, take other mitigation actions, and/or for evacuations.

Table 17. Comparison of Figure of Merit Results for Unmitigated SBO – Difference in Timing

Figure of merit	Scenario 1 STSBO	Scenario 2 LTSBO – 8h	Scenario 3 LTSBO – 16h
0.5 kg of H_2 is generated[a]	39	69	31
First fuel failure (gap release)[a]	4	8	7
100 kg of H_2 is generated[a]	84	188	50
First cladding metal melting[a]	75	177	43
First cladding collapse[a]	79	183	42
Lower head failure[a]	-62	94	-73
Containment failure[a]	-50	152	-14
First deflagration in building[a]	-50	152	-7
0.5 kg noble gas release to environment[a]	-39	151	-15
H_2 gas generated at 32 h[b]	-223	-755	-569
CO gas generated at 32 h[b]	-3757	-11285	-4290

[a] = *minute* [b] = *kg*

Table 18. Comparison of Figure of Merit Results for Unmitigated SBO – Percent Additional Time from Loss of Water Injection

Figure of merit	Scenario 1 STSBO	Scenario 2 LTSBO – 8h	Scenario 3 LTSBO – 16h
0.5 kg of H_2 is generated	56%	14%	9%
First fuel failure (gap release)	6%	2%	2%
100 kg of H_2 is generated	87%	36%	13%
First cladding metal melting	67%	31%	11%
First cladding collapse	71%	33%	11%
Lower head failure	-11%	8%	-9%
Containment failure	-9%	15%	-1%
First deflagration in building	-9%	15%	-1%
0.5 kg noble gas release to environment	-7%	15%	-2%

Table 19 summarizes the difference in figures of merit between the FeCrAl Case 2 and Zircaloy case for the SBO scenarios where these was an extended period of water injection before the loss of the ability to inject water. These scenarios are akin to the scenarios at Fukushima Daiichi Units 2 and 3 in that water injection is maintained for an extended period of time [39, 40]. Table 20 is the percentage difference in timing of the events, of FeCrAl compared to the Zircaloy case, with respect to the timing of loss of water injection.

In both scenarios, FeCrAl provides a substantial gain over Zircaloy for the figures of merit. For many of the figures of merit, the difference in timing is on the order of 1-5 hours or 19-49% of additional time. FeCrAl provides additional time for operators to restore water injection, take other mitigation actions, and/or for evacuations. For Scenario 4 in particular, the accident is stabilized before containment failure for the FeCrAl case in contrast to the Zircaloy case.

Table 19. Comparison of Figure of Merit Results for SBO with Mitigation Loss – Difference in Timing

Figure of merit	Scenario 4 LTSBO – 16h	Scenario 5 LTSBO – 24h
0.5 kg of H_2 is generated[a]	89	101
First fuel failure (gap release)[a]	12	15
100 kg of H_2 is generated[a]	249	290
First cladding metal melting[a]	240	254
First cladding collapse[a]	242	282
Lower head failure[a]	24	*
Containment failure[a]	313	277
First deflagration in building[a]	318	**
0.5 kg noble gas release to environment[a]	315	280
H_2 gas generated at 32 h[b]	-381	***
CO gas generated at 32 h[b]	-2	***

[a] = ***minute*** [b] = ***kg***

*Both the Zircaloy and FeCrAl Case 2 predicts this event does not occur during simulation

**FeCrAl Case 2 predicts this event does not occur during simulation

*** Both the Zircaloy and FeCrAl Case 2 predicts no flammable gas generation by 32 h

Table 20. Comparison of Figure of Merit Results for SBO with Mitigation Loss – Percent Additional Time from Loss of Water Injection

Figure of merit	Scenario 4 LTSBO – 16h	Scenario 5 LTSBO – 24h
0.5 kg of H_2 is generated	20%	19%
First fuel failure (gap release)	3%	3%
100 kg of H_2 is generated	48%	49%
First cladding metal melting	43%	37%
First cladding collapse	43%	41%
Lower head failure	2%	*
Containment failure	47%	39%
First deflagration in building	48%	**
0.5 kg noble gas release to environment	47%	40%

*Both the Zircaloy and FeCrAl Case 2 predicts this event does not occur
**FeCrAl Case 2 predicts this event does not occur

As noted for Scenarios 1-5, FeCrAl can provide additional time for operators to take action during a severe accident to restore water injection. Scenarios 6 and 7 assume water injection is restored after some duration of time and remains active throughout the remainder of the simulation. Table 21 summarizes the difference in figures of merit between the FeCrAl Case 2 and Zircaloy case for the mitigated SBO scenarios.

For the mitigated STSBO, the FeCrAl case substantial quantities of hydrogen are not generated, and the core geometry remains intact. In contrast, the Zircaloy case generates substantial quantities of hydrogen and nearly 86% of the core collapses.

For the mitigated LTSBO, the FeCrAl case is stabilized before containment failure. In contrast, the containment fails in the Zircaloy case leading to deflagrations in the building and releases of radionuclides to the environment. The FeCrAl case also generates approximately 1 ton less hydrogen. Both cases illustrate the potential advantage of a FeCrAl based core over the existing Zircaloy based core with respect to the ability to stabilize a severe accident.

Table 21. Comparison of Figure of Merit Results for Mitigated SBO – Difference in Timing

Figure of merit	Scenario 6 MSTSBO	Scenario 7 MLTSBO
0.5 kg of H_2 is generated[a]	39	69
First fuel failure (gap release)[a]	4	8
100 kg of H_2 is generated[a]	**	188
First cladding metal melting[a]	**	177
First cladding collapse[a]	**	185
Lower head failure[a]	*	*
Containment failure[a]	*	**
First deflagration in building[a]	*	**
0.5 kg noble gas release to environment[a]	*	**
H_2 gas generated at 32 h[b]	-1,354	-1,056
CO gas generated at 32 h[b]	-6	-1

[a] = *minute* [b] = *kg*
*Both the Zircaloy and FeCrAl Case 2 predicted this event does not occur
**FeCrAl Case 2 predicted this event does not occur

5. SUMMARY

Iron-Chromium-Aluminum alloys are under active development as an ATF concept. Its key advantage over Zircaloy is its substantially slower oxidation kinetics up to 1773 K (1500°C). To support further development and future adoption, there is a need to assess the potential gains afforded by the FeCrAl ATF concept.

In order to assess the performance of the FeCrAl ATF concept under severe accident conditions, knowledge of a range of thermophysical and degradation characteristics is needed. The melting point of the FeCrAl metal and the oxide formed in a steam environment were explored experimentally and analytically. The solidus temperatures for the metal alloys given in Table 3 were determined using the thermal arrest method. The oxides of failed FeCrAl specimens showed no DSC peak indicative of melting up to 1700°C in Ar-20%O_2 environment. However, the free poured powders did densify significantly with sample 11501 measured to be ~68% of the theoretical value; so it is possible that liquid did form. However, in the absence of a clear DSC signal, melting onset is indeterminate for the oxides and must be estimated at a much higher temperature than the 1450°C experienced with the SATS test in both UHP Ar and Ar-20%O_2 atmospheres. The results from this work allow for a refinement of the preliminary Fe-Cr-Al and Fe-Cr-Al-O thermodynamic assessments.

A range of station blackout severe accidents were simulated with the MELCOR code. The simulations took into account refined FeCrAl melting points and a refinement of the oxidation rate at high temperatures. Compared to previous work [13], the gains afforded by the FeCrAl ATF concept over the existing Zircaloy system currently in use were predicted to be less. However, FeCrAl provided gains over Zircaloy in most metrics for all scenarios analyzed with respect to timing and flammable gas generation. For unmitigated SBOs, the FeCrAl ATF concept benefits from prolonged boil down of the core. The FeCrAl ATF concept delays the onset of cladding collapse by 75-79 minutes for the STSBO scenario and approximately 3-3.5 hours for the LTSBO scenario with DC power loss at 8 hours. Containment failure occurred 13-50 minutes sooner in the STSBO, however, was delayed 1.5-2.5 hours for the for the LTSBO scenario with DC power loss at 8 hours.

For the two scenarios where water injection was maintained for an extended period of time (16 or 24 hours) before failure, the FeCrAl ATF concept exhibited much higher gains. For example, employing FeCrAl delayed the onset of cladding collapse by 4-4.7 hours and the failure of containment by 4.6-5.2 hours.

The benefit of the delayed accident progression by the FeCrAl ATF concept was exhibited by the two SBO scenarios where water injection was restored after a specified period of time. In both scenarios the accident was stabilized at an earlier time and at an earlier stage for the FeCrAl cases compared to the Zircaloy cases.

Although a range of SBO severe accidents were analyzed that are representative of higher probability severe accident scenarios [37] and the industry's experience with Fukushima Daiichi [39], there are many other possible severe accident scenarios. Other scenarios such as unmitigated LOCAs should be analyzed. In addition, the operator response and the recovery of water injection (if applicable) were prescribed as the same for both the Zircaloy and FeCrAl cases analyzed. The benefit of a delayed accident progression for operator actions (both on opportunity and success probability) or the lack of deflagrations influencing accident response was not accounted for in the analyses. Finally, assessments using other severe accident modeling tools, such a MAAP, should be pursued given the known differences between the codes [42].

There is still a need for additional information on the high temperature degradation characteristics of FeCrAl cladding and channel boxes. The existing Zircaloy system is supported by a range of fuel bundle tests [30]. These tests with Zircaloy provide confidence in the predictions by codes such as MELCOR. However, this database is currently absent for FeCrAl. Tests such as those conducted at the QUENCH facility are needed. Other information, such as that from burst testing [34], is underway. The additional information needs include knowledge of the possible eutectics formed during degradation, the failure points of the oxides under prototypic conditions, and the relocation characteristics of the collapsed fuel

rods. In addition to in-vessel characteristics, further analysis is need in the behavior of FeCrAl during the ex-vessel portion of the accident progression with respect to MCCI and the possibility for fuel-coolant interactions. Finally a fuel assembly design has been developed and analyzed accounting for thermal-hydraulic, neutronic, fuel-performance, economic considerations, and accident performance.

Notwithstanding future work, the current analyses continue to suggest that the FeCrAl ATF concept would provide enhanced accident tolerance for a BWR during station blackout severe accidents.

REFERENCES

1. F. Goldner, “Development Strategy for Advanced LWR Fuels with Enhanced Accident Tolerance,” Enhanced Accident Tolerant LWR Fuels National Metrics Workshop, Germantown, MD, October 2012.
2. K. A. Terrani, S. J. Zinkle, L. L. Snead, “Advanced Oxidation Resistant Iron-Based Alloys for LWR Fuel Cladding,” J. Nuc. Mat. 448(1–3), pp. 420–435 (2014).
3. M. Snead, et. al., “Technology Implementation Plan ATF FeCrAl Cladding for LWR Application,” ORNL/TM-2014/353, May 2015.
4. L. J. Ott, K. R. Robb, D. Wang, “Preliminary assessment of accident-tolerant fuels on LWR performance during normal operation and under DB and BDB accident conditions,” J. Nuc. Mat., 448(1–3), pp.520–533 (2014).
5. K. A. Terrani, D. Wang, L. J. Ott, and R. O. Montgomery, "The effect of fuel thermal conductivity on the behavior of LWR cores during loss-of-coolant accidents," J. Nuc. Mat., 448(1–3), pp.512–519 (2014).
6. B. J. Merril and S. M. Bragg-Sitton, “Status Report on Advanced Cladding Modeling Work to Assess Cladding Performance Under Accident Conditions,” INL/EXT-13-30206, September 2013.
7. N. R. Brown, et al. "Neutronic evaluation of a PWR with fully ceramic microencapsulated fuel. Part II: Nodal core calculations and preliminary study of thermal hydraulic feedback." Annals of Nuclear Energy 62 (2013): 548-557.
8. L. Y. Cheng, A. Cuadra, and N. Brown, “PWR Plant Model to Assess Performance of Accident Tolerant Fuel in Anticipated Transients and Accidents,” No. BNL--107113-2014-CP, Brookhaven National Laboratory, 2014.
9. M. T. Farmer, L. Leibowitz, K. A. Terrani, and K. R. Robb, “Scoping Assessments of ATF Impact on Late Stage Accident Progression Including Molten Core-Concrete Interaction,” J. Nuc. Mat., 448(1–3), pp.534–540 (2014).
10. N. R. Brown, M. Todosow, A. Cuadra, "Screening of advanced cladding materials and UN–U_3Si_5 fuel," Journal of Nuclear Materials 462 (2015): 26-42.
11. S. Bragg-Sitton, B. Merrill, M. Teague, L. Ott, K. Robb, M. Farmer, M. Billone, R. Montgomery, M. Todosow, and C. Stanek, “Advanced Fuels Campaign Light Water Reactor Accident Tolerant Fuel Performance Metrics,” INL/EXT-13-29957, FCRD-FUEL-2013-000264, February 2014.
12. X. Wu, et al, “Preliminary Safety Analysis of PWR with Accident-Tolerant Fuel during Severe Accident Conditions,” Annals of Nuc. Energy, 80, pp.1–13 (2015).
13. K. R. Robb, “Analysis of the FeCrAl Accident Tolerant Fuel Concept Benefits During BWR Station Blackout Accidents,” Proc. of NURETH-16, Chicago, IL, USA, August 30-September 4, 2015.
14. Sandia National Laboratories, MELCOR Computer Code Manuals, Version 1.8.6, NUREG/CR-6119, Rev. 3, September 2005.
15. Sandvik AB, “Kantahl APM (tube)” datasheet, updated August, 8 2012, http://www.kanthal.com/en/products/material-datasheets/tube/kanthal-apm/, accessed 6/8/2016.
16. Sandvik AB, “Kantahl APMT (tube)” datasheet, updated August, 8 2012, http://www.kanthal.com/en/products/material-datasheets/tube/kanthal-apmt/, accessed 6/8/2016.
17. K. W. Kang, J. H. Yang, J. H. Kim, Y. W. Rhee, D. J. Kim, K. S. Kim, K. W. Song, Thermochim. Acta, 455 (1) (2007) 134-7.
18. L. Kjellqvist, M. Selleby, B. Sundman, CALPHAD, 32 (3) (2008) 577-92.
19. I. Ansara, M. Rand, A. Dinsdale, Thermochemical database for light metal alloys, 2, (1998).
20. Saltykov, O. Fabrichnaya, J. Golczewski, F. Aldinger, J. Alloys Compd., 381 (1) (2004) 99-113.
21. A. Muan, C. Gee, J. Am. Ceram. Soc., 39 (6) (1956) 207-14.
22. D. Shishin, V. Prostakova, E. Jak, S. A. Decterov, Metallurgical and Materials Transactions B, 47 (1) (2016) 397-424.
23. C. Bale, P. Chartrand, S. Degterov, G. Eriksson, K. Hack, R. B. Mahfoud, J. Melançon, A. Pelton, S. Petersen, CALPHAD, 26 (2) (2002) 189-228.

24. K. R. Robb, “Updated Peach Bottom Model for MELCOR 1.8.6: Description and Comparisons,” ORNL/TM-2014/207, September 2014.
25. B. A. Pint, K. A. Terrani, Y. Yamamoto, and L. L. Snead, “Material Selection for Accident Tolerant Fuel Cladding,” Metallurgical and Materials Transactions E, September 2015, Volume 2, Issue 3, pp 190-196.
26. J. J. Powers, N. M. George, A. Worrall, and K. A. Terrani, “Reactor Physics Assessment of Alternate Cladding Materials,” Transactions of the 2014 Water Reactor Fuel Performance Meeting / Top Fuel / LWR Fuel Performance Meeting (WRFPM2014/TopFuel 2014), Sendai, Japan, September 14–17, 2014.
27. N. M. George, K. A. Terrani, J. J. Powers, A. Worrall, and G. I. Maldonado, “Neutronic Analysis of Candidate Accident-Tolerant Cladding Concepts in Pressurized Water Reactors,” Annals of N. E., 75, 703–712 (2015).
28. N. M. George, J. J. Powers, G. I. Maldonado, K. A. Terrani, and A. Worrall, “Neutronic Analysis of Candidate Accident-tolerant Cladding Concepts in Light Water Reactors,” Transactions of the American Nuclear Society, 111 (2014) 1363–1366.
29. N. M. George, J. J. Powers, G. I. Maldonado, A. Worrall, and K. A. Terrani, “Demonstration of a Full-core Reactivity Equivalence for FeCrAl Enhanced Accident Tolerant Fuel in BWRs,” Proc. of Advances in Nuclear Fuel Management V (ANFM V), Hilton Head Island, South Carolina, USA, March 29 – April 1, 2015.
30. J. Rempe, M. Farmer, M. Corradini, L. Ott, R. Gauntt, D. Powers, “Revisiting Insights from Three Mile Island Unit 2 Postaccident Examinations and Evaluations in View of the Fukushima Daiichi Accident,” J. Nuc. Sci. and Eng. 172, pp. 223–248 (2012).
31. S. V. Bechta, et. al., “Phase diagram of the UO_2–FeO_{1+x} system,” J. of Nuclear Materials, 362, pp 46-52, 2007.
32. M. Barrachin, D. Gavillet, R. Dubourg, A. De Bremaecker, “Fuel and fission product behaviour in early phases of a severe accident. Part I: Experimental results of the PHEBUS FPT2 test,” J. of Nuclear Materials, 453, pp 340-354, 2014.
33. P. Pacenti, et. al., Dissolution of UO_2 by FeO melts, Corium Interaction and Thermochemistry, Interim Report” European Commission Joint Research Centre, Environment Institute, EUR 18661 EN, , 1998.
34. C. P. Massey, K. A. Terrani, S. N. Dryepondt, B. A. Pint, “Cladding Burst Behavior of Fe-based Alloys Under LOCA,” J. Nuclear Materials, 470, pp 128-138, 2016.
35. Sandia National Laboratories, MELCOR Computer Code Manuals, Version 2.1, NUREG/CR-6119, Rev. 4, September 2008, Draft.
36. K. R. Robb, M. T. Farmer, M. W. Francis, “Ex-Vessel Core Melt Modeling Comparison between MELTSPREAD-CORQUENCH and MELCOR 2.1,” ORNL/TM-2014/1, March 2014.
37. US Nuclear Regulatory Commission, “State-of-the-Art Reactor Consequence Analyses Project; Volume 1: Peach Bottom Integrated Analysis,” NUREG/CR-7110, Vol. 1, January 2012.
38. US Nuclear Regulatory Commission, “Severe accident risks: an assessment for five US nuclear power plants, NUREG-1150,” US Nuclear Regulatory Commission, Washington, DC, 1990.
39. Nuclear Emergency Response Headquarters, Government of Japan, “Report of Japanese Government to the IAEA Ministerial Conference on Nuclear Safety — The Accident at TEPCO’s Fukushima Nuclear Power Stations,” June 2011.
40. R.O. Gauntt, et. al., “Fukushima Daiichi Accident Study (Status as of April 2012),” SAND2012-6173, June 2012.
41. M. Farmer, et. al., “Reactor Safety Gap Evaluation of Accident Tolerant Components and Severe Accident Analysis,” ANL/NE-15/4, March 31, 2015.
42. D. Luxat, J. Hanophy, D. Kalanich, R. Wachowiak, “Modular Accident Analysis Program (MAAP) – MELCOR Crosswalk: Phase 1 Study,” EPRI report 3002004449, November 2015.